Universitat Politècnica de Catalunya
Facultat de Matemàtiques i Estadística

Master in Advanced Mathematics and Mathematical Engineering

Master's thesis

Modelling the homeostasis of intestinal organoids

Josep Bataller i Umbert

Supervised by Marino Arroyo Balaguer

June, 2022

I would like to thank Marino Arroyo and Alejandro Torres for their support all these months. They have always been available for me to discuss all the issues that have emerged and encouraged me to progress in the project.

I would also like to thank Xavier Trepat, Marija Matejcic and Gerardo Ceada, from the *Institut de Bioenginyeria de Catalunya* (IBEC), for the insightful discussions on the biological aspects of the thesis.

Abstract

Homeostasis is a process by which biological systems maintain stability in an evolving environment. However, homeostasis is far from being a static state. In rapidly self-renewing tissues such as the small intestine epithelium, most cells are replaced every few days, and during their lifespan undergo differentiation and migrate over long distances along gradients of cell shape and density. How physical aspects integrate with biological phenomena to give rise to this dynamical self-organized state is not understood. To address this, we model mathematically and computationally intestinal organoids, a simpler in-vitro system with great accessibility, geometric simplicity, and yet capturing the essential features of intestinal homeostasis. To model this system, we adopt a continuum hydrodynamic model where the system is described in terms of the cell number density and the concentration of morphogen Wnt. Conservation and mechanical partial differential equations control the dynamics of these variables. We provide a systematic derivation of the model, its numerical discretization, and examine its ability to self-organize into dynamical steady-states, which closely mimic the experimental observations in terms of cell density fields, velocity fields and division/extrusion patterns. We further study the sensitivity of the homeostatic steady-states on different model parameters. Our work thus provides a framework to quantitatively understand and control homeostasis in intestinal organoids.

Keywords

Intestinal organoids, mathematical modelling, partial differential equations, finite elements, dimensional analysis.

Contents

1 Introduction **3**

2 Governing equations **4**

2.1 System of equations 4

2.2 Onsager's derivation 6

2.3 Dimensional analysis 8

3 Numerical implementation **11**

3.1 Weak form of the problem 11

3.2 Galerkin discretization 12

3.3 Time discretization 13

3.4 Parameters 15

4 Results **16**

4.1 Convergence analysis 16

4.2 Homeostatic steady state 17

4.3 Initial conditions 18

4.4 Effect of the parameters 21

4.5 Importance of degradation 28

4.6 Cell divisions, cell extrusions and Wnt generation 29

5 Conclusions **32**

6 Future work **33**

A Extra terms in the momentum equation **34**

B Adaptative stepsize **35**

1. Introduction

The small intestine is a very dynamic system, where cells are in continuous self-renewal and migration. Homeostatis is the process by which these kind of systems maintain stability in an evolving environment. Far from being static, homeostasis is a very dynamic process. Epithelium cells undergo differentiation and migration over long distances along gradients of cell density. The coupling between the physical and biological aspects in the small intestine is not fully understood, but measuring physical variables in an in-vivo environment is a very difficult task. Instead, a simpler in-vitro system is created, the intestinal organoids [1]. These systems are much more accessible, they have simple geometries and, what's more important, they conserve the main features of intestinal homeostasis. Physical measurements, such as cell densities and velocity fields, can be performed in intestinal organoids in a much simpler way, as well as maps of morphogens, and we have control over the geometric confinement of other physical quantities. Hence, these are great systems to be coupled with a mathematical model to describe them [2].

Tissue homeostasis in intestinal organoids results from the interaction between signalling pathways and mechanical cues [3, 4]. The organoid is mostly formed by three different cell types. Firstly, there are the stem cells. These cells proliferate and differentiate, giving rise to other types of cells. Secondly, there are the paneth cells, which act as master regulators of the division and differentiation of nearby cells. They do so by segregating certain proteins which regulate the differentiation of stem cells. Finally, there are the intestinal absorptive cells (or enterocytes), which are the cells responsible of nutrient absorption in the small intestine. These cells are eventually extruded from the tissue after a certain time [5–7].

These cells organize in space in two regions, the crypts and the villi. The crypt is formed by stem and paneth cells, where division happens, whereas enterocytes differentiate from stem cells as they leave the crypt (probably driven by a gradient of tension because of the high packing caused by cell division [8]) and travel to villus-like regions where they are extruded. In the villi, neither stem nor paneth cells are present, and these are the regions where nutrient absorption takes place in the small intestine.

The process by which cells differentiate and migrate towards the villi is regulated by two main signalling pathways, which subsequently activate each other:

- **Wnt** : Wnt ligands are secreted by paneth cells, which bind Frizzled (FZD) receptors on neighbouring cells [10]. This in turn leads to an accumulation of β-catenin in the cytoplasm, which eventually translocates to the nucleus and regulates the transcription of genes that ensure cell stemness. Wnt dilutes because of cell divisions of stem cells, and because the daughter cells move away from the source generated by paneth cells. This dilution eventually leads to differentiation of stem cells into enterocytes. The levels of β-catenin through Wnt control the expression of different EphB (high Wnt) and EphrinB (low Wnt) ligands. The differential adhesion between EphB-EphrinB has been proposed as a mechanism for cell sorting [11]. Paneth cells express ephB3 ligands, which ensure they stay close to stem cells.

- **Notch** : Similarly to Wnt, Notch is produced by paneth cells and also binds receptors of neighbouring cells [9]. Notch signalling antagonises the transcription of Math1, which control the differentiation into secretory cells, and in particular into paneth cells. When stem cells differentiate into paneth cells, then these travel to the crypt centre presumably following the gradient of Eph.

The goal of this thesis is to describe the governing cell and morphogen transport, as well as the tissue dynamcis, of intestinal organoids by means of a mathematical model, consisting on a coupled set of partial differential equations. Wnt is considered to be the determining signaling pathway for cell differentiation,

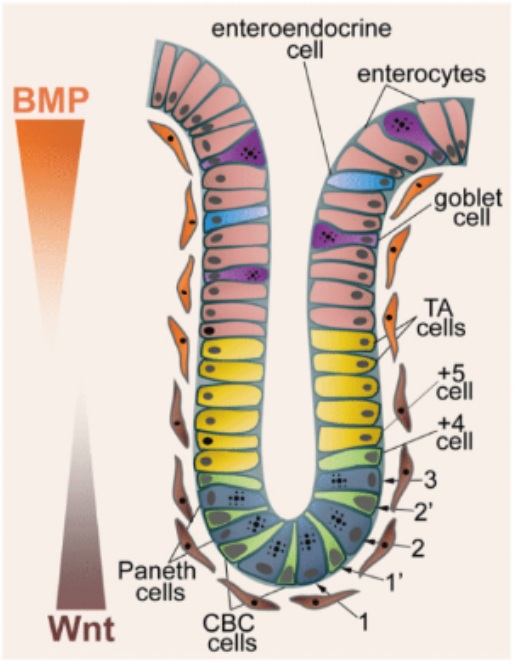

Figure 1: Cellular architecture in the crypt of the small intestine (image taken from [9]).

neglecting the effect of Notch, to reduce the complexity of the model. In that way, the dynamics of the model are determined by three variables: the cell density, the concentration of Wnt and the velocity of advection of the cells. The cells are assumed to be stem cells when the Wnt concentration in that region is over a certain threshold, and when the Wnt concentration decreases bellow that threshold the cells become enterocytes.

2. Governing equations

2.1 System of equations

First of all we need to define the governing equations of the system. We will deduce them in two dimensions, since the experimental setup is a cell sheet, although most of our study will be performed in one dimension for simplicity. The simplification from one model to the other is straightforward.

We describe the state of the system with the cell density ρ, measuring the number of cells per unit volume, and the concentration of a signalling molecule per cell, c, representing Wnt signalling in the crypt. We can assume that c effectively characterises the cell state (stem or enterocyte): if $c > c^*$ the cell is a stem cell, if $c < c^*$ the cell is an enterocyte. The cells move with a velocity field $\mathbf{v}$.

Conservation of the number of cells can be expressed in terms of a continuity equation

$$\partial_t \rho + \nabla \cdot (\rho \mathbf{v}) = k_d(c, \rho)\rho - k_e(c)\rho, \tag{1}$$

where the left-hand side stems from conservation of cells in the absence of cell divisions or extrusions. The first term in the right-hand side characterises divisions, which happen with a rate $k_d(c, \rho)$, which depends

both on c and on ρ. The second term in the right-hand side characterises extrusions, which happen with a rate $k_e(c)$. Through the dependence on c and ρ, we can model the different division and extrusion rates of stem cell and enterocytes. More precisely, we expect divisions to take place at high concentrations of Wnt (stem cells) and small values of the density (otherwise they are too packed and they cannot divide). Instead, extrusions take place at small Wnt concentrations (enterocytes).

Observe the difference between the left-hand side terms between the conservation equation and the transport equation. This difference arises from the fact that c is a concentration, which is in units of number of molecules per cell, while ρ is in units of cells per unit area. Hence, when there is a flux with $\nabla \cdot \mathbf{v} \neq 0$ which compacts the cells, ρ has to change accordingly. On the contrary, c does not change due to this effect, so there is no term $c\nabla \cdot \mathbf{v}$ in the transport equation.

Similarly, conservation of the signalling molecule c can be expressed in terms of a transport equation,

$$\partial_t c + \nabla c \cdot \mathbf{v} = k_p(\rho_p) - \frac{1}{2} k_d(c, \rho) c - k_n c, \tag{2}$$

where k_n is the rate of degradation of Wnt [12] and $k_p(\rho_p)$ characterises the attachment of Wnt to Fz ligands next to a Paneth cell, characterised by the Paneth cell density ρ_p; for now we take ρ_p as given. Every time a cell divides, it splits its Wnt-ligands to its daughters, which leads to the term $-k_d(c, \rho)c/2$.

Finally, we need an equation for momentum balance that tells us how $\mathbf{v}$ behaves. In the absence of inertia (because the system operates at very low Re numbers), we can write

$$\nabla \cdot \boldsymbol{\sigma} + \mathbf{b} = \mathbf{0}, \tag{3}$$

where $\boldsymbol{\sigma}$ is the stress tensor (with units of force divided by length in 2D, and units of force if the system is 1D), and $\mathbf{b}$ is a body force. We can consider that

$$\boldsymbol{\sigma} = \boldsymbol{\sigma}^e + \boldsymbol{\sigma}^v, \tag{4}$$

where $\boldsymbol{\sigma}^e$ is an elastic stress and $\boldsymbol{\sigma}^v$ is a viscous stress. Some other terms could be added as well (see appendix A). The elastic stress is going to be isotropic [13], $\boldsymbol{\sigma}^e = \sigma^e \mathbf{I}$, with σ^e a tension and $\mathbf{I}$ the identity. We define the elastic energy

$$\mathcal{F}_{\text{ela}} = \int_\Omega f(\rho; c) d\Omega, \tag{5}$$

where $f(\rho; c)$ is the elastic energy density as a function of ρ, and possibly depending on c parametrically. It can be shown (see 2.2) that tension has the form

$$\sigma^e = \left[f(\rho; c) - f'(\rho; c)\rho \right] \tag{6}$$

In particular, if we consider that $f(\rho) = \frac{k(c)}{2}\left(1 + 2\left(\frac{\rho}{\rho_0(c)}\right)^{3/2}\right)$,

$$\sigma^e = \frac{k(c)}{2}\left[1 - \left(\frac{\rho}{\rho_0(c)}\right)^{3/2}\right]. \tag{7}$$

For simplicity, we can assume that the viscous stress follows a Newtonian rheology,

$$\boldsymbol{\sigma}^v = 2\mu(c)\nabla^S \mathbf{v} \tag{8}$$

where $\nabla^S \mathbf{v} = [\nabla \mathbf{v} + (\nabla \mathbf{v})^T]/2$ is the symmetrised gradient of the velocity (the rate of deformation tensor), and μ is the viscosity per unit density, that can depend on the cell type through c. Finally, for the body forces we consider a friction

$$\mathbf{b} = -\eta(c)\left[\mathbf{v} - \mathbf{v}^*(c)\right], \tag{9}$$

that accounts both for friction with the substrate through η, and possibly for a self-propelling force $\eta(c)\mathbf{v}^*(c)$.

2.2 Onsager's derivation

An alternative to derive the momentum equation is the Onsager's variational formalism. This is a variational formalism for the derivation of thermodynamically consistent non-equilibrium models based on the minimization of a functional, called the Rayleighian, that sets a balance between the rate of change of free energy of the system, the input of energy by external power, and energy dissipation [14, 15]. In this formalism, one needs to characterize the free energy of the system via state variables, such as the density field, the dissipation of the system in the form of a dissipation potential in terms of process variables, such as the velocity, and the power input. This formalism can be written as the following minimization problem:

$$\mathbf{v} = \arg\min_{\mathbf{w}} \mathcal{R}[\mathbf{w}; \rho, c] \tag{10}$$

where $\mathcal{R}$ is the Rayleighian

$$\mathcal{R}[\mathbf{v}; \rho, c] = \dot{\mathcal{F}}[\mathbf{v}; \rho, c] + \mathcal{D}[\mathbf{v}; \rho, c], \tag{11}$$

In this equation, $\mathcal{F}$ is the free energy, here $\mathcal{F}[\rho, c] = \int_\Omega f(\rho; c) d\Omega$, and $\mathcal{D}$ is the dissipation potential, $\mathcal{D} = \int_\Omega \left[\mu(c)|\nabla^S \mathbf{v}|^2 + \frac{1}{2}\eta(c)\left(\mathbf{v} - \mathbf{v}^*(c)\right)^2\right] d\Omega$. To compute $\dot{\mathcal{F}}$ one needs to compute the material time derivative of $\mathcal{F}$ using Reynold's transport theorem and then substitute the transport equations for $\partial_t \rho$ and $\partial_t c$.

Let's check that this Rayleighian gives rise to the equations of the system (Eq. 3). We start by computing $\dot{\mathcal{F}}$. If we apply Reynold's transport theorem, together with the transport equations, we obtain:

$$\frac{d}{dt}\mathcal{F}(\rho, c) = \frac{d}{dt}\int_\Omega f(\rho, x) d\Omega = \int_\Omega \frac{d}{dt} f(\rho, c) + \nabla \cdot (f\mathbf{v}) d\Omega$$

$$\frac{d}{dt} f(\rho, c) = f_\rho(\rho, c)\rho_t + f_c(\rho, c)c_t$$

$$\frac{d}{dt} f(\rho, c) = f_\rho(\rho, c)(k_d(\rho, c)\rho - k_e(c)\rho - \nabla \cdot (\rho \mathbf{v})) + f_c(\rho, c)(k_p(c) - \frac{1}{2}k_d(\rho, c)c - k_n c - \nabla c \cdot \mathbf{v})$$

We have used the notation $\frac{d}{d\rho} f = f_\rho$ (and similarly for f with respect to c and ρ and c with respect to t). For convenience, from now on we will not write the explicit dependence of f with respect to ρ and c, nor the dependence of k_e, k_d and k_p with respect to ρ, c or ρ_p. When considering the variational analysis only the terms with contributions of $\mathbf{v}$ will appear in the final expression when minimizing the Rayleighian. Hence, we can omit the terms which do not have dependency with respect to $\mathbf{v}$.

$$\frac{d}{dt} f = -f_\rho \nabla \cdot (\rho \mathbf{v}) - f_c \nabla c \cdot \mathbf{v}$$

$$\frac{d}{dt}\mathcal{F}(\rho, c) = \int_\Omega \left[-f_\rho \nabla \cdot (\rho \mathbf{v}) - f_c \nabla c \cdot \mathbf{v} + \nabla \cdot (f\mathbf{v})\right] d\Omega$$

$$\frac{d}{dt}\mathcal{F}(\rho, c) = \int_\Omega \left[-f_\rho \nabla \rho \cdot \mathbf{v} - f_\rho \rho \nabla \cdot \mathbf{v} - f_c \nabla c \cdot \mathbf{v} + \nabla f \cdot \mathbf{v} + f \nabla \cdot \mathbf{v}\right] d\Omega$$

$$\frac{d}{dt}\mathcal{F}(\rho, c) = \int_\Omega \left[(-f_\rho \nabla \rho - f_c \nabla c + \nabla f) \cdot \mathbf{v} + (-f_\rho \rho + f) \nabla \cdot \mathbf{v}\right] d\Omega$$

The term multiplying $\mathbf{v}$ in the integral is zero (applying the chain rule to ∇f). If we apply integration by parts to the second term we obtain:

$$\frac{d}{dt}\mathcal{F}(\rho, c) = -\int_\Omega \nabla(-f_\rho \rho + f) \cdot \mathbf{v} d\Omega = -\int_\Omega \nabla \cdot ((-f_\rho \rho + f)\mathbf{I}) \cdot \mathbf{v} d\Omega$$

Let's compute now the minimum of the Rayleighian. The way to do so is to consider:

$$\frac{d}{d\epsilon}\mathcal{R}[\mathbf{v} + \epsilon \mathbf{w}; \rho, c]_{\epsilon=0} = 0$$

$$\mathcal{R}[\mathbf{v} + \epsilon \mathbf{w}; \rho, c] =$$

$$\int_\Omega \left[-\nabla \cdot ((-f_\rho \rho + f)\mathbf{I}) \cdot (\mathbf{v} + \epsilon \mathbf{w}) + \mu(c)|\nabla^S(\mathbf{v} + \epsilon \mathbf{w})|^2 + \frac{1}{2}\eta(c)\left(\mathbf{v} + \epsilon \mathbf{w} - \mathbf{v}^*(c)\right)^2\right] d\Omega$$

$$\frac{d}{d\epsilon}\mathcal{R}[\mathbf{v} + \epsilon \mathbf{w}; \rho, c]_{\epsilon=0} =$$

$$\int_\Omega \left[-\nabla \cdot ((-f_\rho \rho + f)\mathbf{I}) \cdot \mathbf{w} + 2\mu(c)\nabla^S \mathbf{v}^T \cdot \nabla^S \mathbf{w} + \eta(c)(\mathbf{v} - \mathbf{v}^*(c))^T \cdot \mathbf{w}\right] d\Omega$$

$$\frac{d}{d\epsilon}\mathcal{R}[\mathbf{v} + \epsilon \mathbf{w}; \rho, c]_{\epsilon=0} =$$

$$\int_\Omega \left[-\nabla \cdot ((-f_\rho \rho + f)\mathbf{I}) \cdot \mathbf{w} - \nabla \cdot (2\mu(c)\nabla^S \mathbf{v}^T)\mathbf{w} + \eta(c)(\mathbf{v} - \mathbf{v}^*(c))^T \cdot \mathbf{w}\right] d\Omega = 0$$

Observe that this is precisely the weak form of the momentum balance equation. Since this is true for all functions $\mathbf{w}$, we can recover the strong form of the problem:

$$\nabla \cdot ((-f_\rho \rho + f)\mathbf{I}) + \nabla \cdot (2\mu(c)\nabla^S \mathbf{v}) - \eta(c)(\mathbf{v} - \mathbf{v}^*(c)) = 0$$

Recalling the definitions in Eq. 6, 8 and 9 we recover Eq. 3, which is the strong form of our problem.

2.3 Dimensional analysis

The set of constitutive equations for our model is:

$$\begin{cases} \partial_t \rho + \nabla \cdot (\rho \mathbf{v}) = k_d(c,\rho)\rho - k_e(c)\rho \\ \partial_t c + \nabla c \cdot \mathbf{v} = k_p(\rho_p) - \frac{1}{2} k_d(c,\rho) c - k_n c \\ \nabla \cdot \left(\frac{k(c)}{2} \left[1 - \left(\frac{\rho}{\rho_0(c)} \right)^{3/2} \right] \mathbf{I} \right) + \nabla \cdot (2\mu(c) \nabla^S \mathbf{v}) - \eta(c)(\mathbf{v} - \mathbf{v}^*(c)) = 0 \end{cases} \tag{12}$$

There are several functions depending on c, ρ or ρ_p which need to be specified. Since c is adimensional, we consider that the threshold value between the crypt and the villus is $c^* = c_d$ (so $c < c_d$ at the villus and $c > c_d$ at the crypt). c_d is related to the rate of division of the cells, so that cells divide when $c > c_d$ (they are stem cells) and they stop dividing when $c < c_d$ (they are enterocytes).

To start with, for simplicity, we assume that $\mu(c) = \mu$ and $\eta(c) = \eta$ are constant (they do not depend on the type of cell), and we consider that $\mathbf{v}^*(c) = 0$. As for the rest of the magnitudes:

- **Division rate:**

$$k_d(c,\rho) = \bar{k_d} f_d(c,\rho) = \bar{k_d} \cdot \frac{1 + \tanh \frac{5}{c_d}(c - c_d)}{2} \cdot \frac{\epsilon}{\frac{\rho}{\rho_0} + \epsilon} \tag{13}$$

  Hence, $k_d(c,\rho)$ has a logistic relation with respect to c, so that when $c \to 0$, $k_d \to 0$, and when $c \to 1$, $k_d \to \bar{k_d}$. The term $\frac{\epsilon}{\frac{\rho}{\rho_0} + \epsilon}$ tends to 0 when ρ is much larger than ρ_0, so that for very large concentrations division cannot take place, and it tends to 1 when ρ is very small compared to ρ_0. Note that this expression can also be rewritten as

$$k_d(c,\rho) = \hat{k_d} \cdot \frac{1 + \tanh \frac{5}{c_d}(c - c_d)}{2} \cdot \frac{1}{\frac{\rho}{\rho_0} + \epsilon}$$

  for $\hat{k_d} = \bar{k_d}\epsilon$. In simulations we usually work with this last notation, but both formulations are equivalent except for a change of the values of the parameters.

- **Extrusion rate:**

$$k_e(c) = \bar{k_e} f_e(c) = \bar{k_e} \cdot \frac{1 - \tanh \frac{5}{c_d}(c - c_e)}{2} \tag{14}$$

  Hence, $k_e(c)$ has a logistic relation with $1 - c$, so that when $c \to 1$, $k_e \to 0$, and when $c \to 0$, $k_e \to \bar{k_e}$. Observe that the relation with respect to c is the opposite than the one for $k_d(c,\rho)$, since we expect the extrusions to take place in the villus, where c is close to zero, but divisions take place mostly inside the crypt, where c is close to 1.

- **Wnt generation rate:** $k_p(\rho_p)$. We assume that the density of paneth cells is fixed, in order to simplify the model (otherwise we would require an extra equation to model the evolution of ρ_p). Moreover, we assume that the density of Paneth cells is constant in time, since the dynamics of such cells is much slower than the dynamics of stem cells and enterocytes. Hence, ρ_p only has spatial dependence, so we can give the expression for $k_p(\rho_p)$ simply as a function of x:

$$k_p(\rho_p) = k_p(x) = \bar{k_p} f_p(x) = \bar{k_p} e^{-\left(\frac{1}{l_{gauss}}\left(x - \frac{L}{2}\right)\right)^2} \tag{15}$$

where L is the domain size, and l_{gauss} is a characteristic length, such that if $x = \frac{L}{2} + l_{gauss}$, the Paneth cell generation rate decays by a factor $\frac{1}{e}$. Since we assume periodic boundary conditions, we only need to model one crypt, so the generation of Wnt is focused only in one region in space.

- **Stiffness parameter:**

$$k(c) = \bar{k} f_k(c) = \bar{k} \left((1 - 0.7) \frac{1 + \tanh \frac{5}{c_d}(c - c_d)}{2} + 0.7 \right) \tag{16}$$

The expression is analogous to the one for $k_d(c, \rho)$ (neglecting the dependence on ρ), where k has a logistic dependence with respect to c, being maximum at the crypt ($c \to 1$) and minimum at the villus ($c \to 0$). The factor 0.7 is chosen with this value because the stiffness of the villus is approximately 70% the stiffness of the crypt. For simplicity we assume that the threshold concentration is c_d, as well.

- **Reference density:**

$$\rho_0(c) = \rho_0 f_\rho(c) = \rho_0 \left((1 - 0.5) \frac{1 + \tanh \frac{5}{c_d}(c - c_d)}{2} + 0.5 \right) \tag{17}$$

As in the previous case, ρ_0 is maximum at the crypt and minimum at the villus. The factor 0.5 is chosen with this value because the mean density at the villus is approximately half the density at the crypt. For simplicity we assume that the threshold concentration is c_d, as well.

Our goal now is to study which are the relevant parameters from a physical point of view. Most of these parameters are related to one another, so changing one of them may affect the others. The way to determine the relevant magnitudes is to adimensionalize the equations. First of all, we need to define some reference magnitudes:

- $T = \frac{1}{\bar{k_d}}$, which is the inverse of the maximum cell division rate, $\bar{k_d}$. It serves as a reference time. The normalized time is $\bar{t} = \frac{t}{T} = t\bar{k_d}$.
- The domain length, L, serves as a reference length. The normalized distances are $\bar{x} = \frac{x}{L}$, and the normalized gradients are $\bar{\nabla} = L\nabla$.
- $v_0 = \frac{L}{T}$ is a reference velocity. The normalized velocities are $\bar{v} = \frac{v}{v_0}$.
- The **hydrodynamic length**, $l_h = \sqrt{\frac{\mu}{\eta}}$, which is the square root of the ratio between the viscosity coefficient, μ, and the friction coefficient, η. It gives information on how far interactions in one region affect neighbour regions.
- A reference cell density ρ_0, so that $\bar{\rho} = \frac{\rho}{\rho_0}$ is an adimensional density.
- A reference Wnt concentration c_d, which is the concentration threshold for division, so that $\bar{c} = \frac{c}{c_d}$.

Using these reference magnitudes we can now define a set of adimensional parameters. These parameters appear in the model after adimensionalizing it, and we will see that they are the parameters which play a relevant role in the physics of the problem:

- ϵ, which is related to how steep is the increase of the term $\frac{\epsilon\rho}{\frac{\rho}{\rho_0}+\epsilon}$ with respect to ρ.
- $\delta_1 = \frac{\bar{k_e}}{\bar{k_d}}$, which is the ratio between the maximum extrusion rate, $\bar{k_e}$, and the maximum cell division rate, $\bar{k_d}$. It gives information on how fast are the extrusions with respect to divisions.
- $\delta_2 = \frac{c_e}{c_d}$, which is the ratio between the concentration threshold for extrusion, c_e, and the concentration threshold for division, c_d. Usually $\delta_2 < 1$. We expect to see a very clear separation between the crypt, where divisions dominate, and the villus, where extrusions dominate, when δ_2 is small.
- $\delta_3 = \frac{\bar{k_p}}{\bar{k_d}}$, which is the ratio between the maximum Paneth cell generation rate, $\bar{k_p}$, and the maximum cell division rate, $\bar{k_d}$. It gives information on how fast the Wnt i segregated with respect to the rate of cell division.
- $\delta_4 = \frac{k_n}{\bar{k_d}}$, which is the ratio between the degradation rate and the maximum cell division rate, $\bar{k_d}$. It gives information on how fast the Wnt degradates with respect to the rate of cell division.
- $\ell = \frac{l_{gauss}}{L}$, which is the ratio between the width of the Paneth cells source, l_{gauss} and the length of the domain, L.
- $\ell_h = \left(\frac{L}{l_h}\right)^2 = \frac{\eta}{\mu}L^2$, which is the ratio between the hydrodynamic length, l_h, and the domain size, L.
- $\kappa = \frac{\bar{k}}{2\mu\bar{k_d}}$, which is the ratio between the maximum of the elasticity constant, $\bar{k}$, and the viscosity coefficient, μ, times the maximum cell division rate, $\bar{k_d}$. It gives information on how important elasticity is compared to viscosity.

With all these parameters, the equations can be rewritten as:

- **Continuity equation**: If we multiply by T and divide by ρ_0, the equation becomes:

$$\partial_t \rho \frac{T}{\rho_0} + L\nabla \cdot \left(\frac{\rho}{\rho_0}\frac{T\mathbf{v}}{L}\right) = k_d(c,\rho)T\frac{\rho}{\rho_0} - k_e(c)T\frac{\rho}{\rho_0} \tag{18}$$

$$\partial_{\bar{t}}\bar{\rho} + \bar{\nabla}\cdot(\bar{\rho}\bar{\mathbf{v}}) = f_d(\bar{\rho},\bar{c})\bar{\rho} - \delta_1 f_e(\bar{c})\bar{\rho} \tag{19}$$

- **Transport equation**: If we multiply by T and divide by c_d, the equation becomes:

$$\partial_t c\frac{T}{c_d} + L\nabla\frac{c}{c_d}\cdot\mathbf{v}\frac{T}{L} = k_p(\rho_p)\frac{T}{c_d} - \frac{1}{2}k_d(c)c\frac{T}{c_d} - k_n c\frac{T}{c_d} \tag{20}$$

$$\partial_{\bar{t}}\bar{c} + \bar{\nabla}\bar{c}\cdot\bar{\mathbf{v}} = \delta_3 f_p(x) - \frac{1}{2}f_d(\bar{c})\bar{c} - \delta_4\bar{c} \tag{21}$$

- **Momentum balance**: If we multiply by L and T and divide by μ, the equation becomes:

$$L\nabla\cdot\left(\frac{k(c)T}{2\mu}\left[1-\left(\frac{\rho}{\rho_0(c)}\right)^{3/2}\right]\right) + L\nabla\cdot\left(2L\nabla^S\mathbf{v}\frac{T}{L}\right) - \frac{\eta}{\mu}L^2\mathbf{v}\frac{T}{L} = 0 \tag{22}$$

$$\bar{\nabla}\cdot\left(\kappa f_k(\bar{c})\left[1-\left(\frac{\bar{\rho}}{f_\rho(\bar{c})}\right)^{3/2}\right]\right) + \bar{\nabla}\cdot(2\bar{\nabla}^S\bar{\mathbf{v}}) - \ell_h\bar{\mathbf{v}} = 0 \tag{23}$$

As for the rest of the expressions which depend on c, ρ and ρ_p, they can also be rewritten as:

- $k_d(c,\rho) = \bar{k_d} f_d(c,\rho) = \bar{k_d}\left(\frac{1+\tanh\frac{5}{c_d}(c-c_d)}{2}\right)\frac{\epsilon}{\frac{\rho}{\rho_0}+\epsilon} = \bar{k_d}\left(\frac{1+\tanh 5(\bar{c}-1)}{2}\right)\frac{\epsilon}{\bar{\rho}+\epsilon}$
- $k_e(c) = \bar{k_e} f_e(c) = \bar{k_e}\left(\frac{1-\tanh\frac{5}{c_d}(c-c_e)}{2}\right) = \bar{k_e}\left(\frac{1-\tanh 5(\bar{c}-\delta_2)}{2}\right)$
- $k_p(\rho_p) = k_p(x) = \bar{k_p} f_p(x) = \bar{k_p} e^{-\left(\frac{1}{l_{gauss}}(x-\frac{L}{2})\right)^2} = \bar{k_p} e^{-\left(\frac{1}{\ell}(\bar{x}-0.5)\right)^2}$
- $k(c) = \bar{k} f_k(c) = \bar{k}\left((1-0.7)\frac{1+\tanh\frac{5}{c_d}(c-c_d)}{2}+0.7\right) = \bar{k}\left((1-0.7)\frac{1+\tanh 5(\bar{c}-1)}{2}+0.7\right)$
- $\rho_0(c) = \rho_0 f_\rho(c) = \rho_0\left((1-0.5)\frac{1+\tanh 5(\bar{c}-1)}{2}+0.5\right)$

3. Numerical implementation

3.1 Weak form of the problem

From now on we will work with our governing equations in adimensional form. Moreover, we will restrict to the one-dimensional case. That is, we have the following set of three equations:

$$\begin{cases} \partial_{\bar{t}}\bar{\rho} + \partial_{\bar{x}}\left(\bar{\rho}\bar{\mathbf{v}}\right) = f_d(\bar{\rho},\bar{c})\bar{\rho} - \delta_1 f_e(\bar{c})\bar{\rho} \\ \partial_{\bar{t}}\bar{c} + \partial_{\bar{x}}\bar{c}\bar{\mathbf{v}} = \delta_3 f_p(x) - \frac{1}{2} f_d(\bar{\rho},\bar{c})\bar{c} - \delta_4\bar{c} \\ \partial_{\bar{x}}\left(\kappa f_k(\bar{c})\left[1-\left(\frac{\bar{\rho}}{f_\rho(\bar{c})}\right)^{3/2}\right]\right) + \partial_{\bar{x}\bar{x}}(2\bar{\mathbf{v}}) - \ell_h\bar{\mathbf{v}} = 0 \end{cases} \tag{24}$$

These equations are defined in a domain $\Omega = (0, L)$ (which after adimensionalization is $\bar{\Omega} = (0,1)$) with periodic boundary conditions. Periodic boundary conditions are satisfied automatically when solving the system without the need to impose any additional condition in the derivation of the weak form. In that way, we do not have to worry about them. For convenience, form now on we will drop the bars over each of the variables, although we work with the adimensional variables unless the opposite is said.

In order to solve this system numerically, we will use a Finite Element Method approximation. The first step to implement this method is to consider the weak form of the problem. Consider the first equation and multiply it by a test function $w \in \mathcal{H}_1(\Omega)$, where $\mathcal{H}_1(\Omega) = \{w(x) \in \mathcal{L}_2(\Omega); w'(x) \in \mathcal{L}_2(\Omega)\}$. If we integrate the equation over Ω it becomes:

$$\int_\Omega \left(w\partial_t\rho + w\partial_x\left(\rho\mathbf{v}\right)\right) d\Omega = \int_\Omega \left(w f_d(\rho,c)\rho - w\delta_1 f_e(c)\rho\right) d\Omega \tag{25}$$

If we integrate by parts and impose periodic boundary conditions (so we can neglect the boundary terms) the equation becomes:

$$\int_\Omega \left(w\partial_t\rho - \partial_x w\rho\mathbf{v}\right) d\Omega = \int_\Omega \left(w f_d(\rho,c)\rho - w\delta_1 f_e(c)\rho\right) d\Omega \tag{26}$$

We can do an analogous derivation with the second and the third equations and we obtain:

$$\int_\Omega (q\partial_t c + q\partial_x c\mathbf{v})\, d\Omega = \int_\Omega \left(\delta_3 q f_p(x) - \frac{1}{2} q f_d(c) c - \delta_4 q c\right) d\Omega \tag{27}$$

$$\int_\Omega \left(\partial_x u \left(\kappa f_k(c)\left[1 - \left(\frac{\bar{\rho}}{f_\rho(c)}\right)^{3/2}\right]\right) + 2\partial_x u \partial_x \mathbf{v} + \ell_h u \mathbf{v}\right) d\Omega = 0 \tag{28}$$

where $q \in \mathcal{H}_1(\Omega)$ and $u \in \mathcal{H}_1(\Omega)$ are the test functions for the second and third governing equations, respectively. Observe that we actually don't require that $q \in \mathcal{H}_1(\Omega)$, since its spatial derivatives don't appear in the weak form, and we only need $q \in \mathcal{L}_2(\Omega)$. However, we can still impose this condition, since it is more restrictive ($q \in \mathcal{H}_1(\Omega) \implies q \in \mathcal{L}_2(\Omega)$), and in practice it does not affect any of the further discussion.

3.2 Galerkin discretization

Once we have the weak form of the problem, the following step is to consider a Galerkin discretization in the spatial domain. That is, we consider a set of basis functions $\{N_i(x)\}_i$, for $i = 1, ..., n_{el}$, with compact support, and consider the following discretization for each of the variables:

$$\rho(x,t) \approx \rho^h(x,t) = \sum_{i=1}^{n_{el}} \rho_i(t) N_i(x) \tag{29}$$

$$c(x,t) \approx c^h(x,t) = \sum_{i=1}^{n_{el}} c_i(t) N_i(x) \tag{30}$$

$$v(x,t) \approx v^h(x,t) = \sum_{i=1}^{n_{el}} v_i(t) N_i(x) \tag{31}$$

For simplicity we have assumed that we discretize all variables in the same space of test functions, and we consider the same elements for each of the variables. This can be modified if the problem presents numerical issues related to stability, but as a first approximation it is good enough. In our simulations we use spline functions of order three. Observe that the temporal depend only affects the coefficients in the sum, since the basis functions are constant in time. With these approximations, and considering the test functions to be $\{N_j(x)\}_j$ as well, with $j = 1, ..., n_{el}$, the weak form becomes:

- **Conservation equation**:

$$\int_\Omega \left(N_j(x)\partial_t \sum_{i=1}^{n_{el}} \rho_i(t) N_i(x) - \partial_x N_j(x) \sum_{i=1}^{n_{el}} \rho_i(t) N_i(x) \sum_{i=1}^{n_{el}} v_i(t) N_i(x)\right) d\Omega =$$

$$\int_\Omega \left(N_j(x) f_d(\sum_{i=1}^{n_{el}} \rho_i(t) N_i(x), \sum_{i=1}^{n_{el}} c_i(t) N_i(x)) \sum_{i=1}^{n_{el}} \rho_i(t) N_i(x)\right) d\Omega -$$

$$\int_\Omega \left(N_j(x)\delta_1 f_e(\sum_{i=1}^{n_{el}} c_i(t) N_i(x)) \sum_{i=1}^{n_{el}} \rho_i(t) N_i(x)\right) d\Omega$$

$$\sum_{i=1}^{n_{el}} \int_\Omega \left(N_j N_i \rho_i'(t) - N_j' N_i \left(\sum_{k=1}^{n_{el}} v_k(t) N_k \right) \rho_i(t) \right) d\Omega$$

$$= \sum_{i=1}^{n_{el}} \left(\int_\Omega N_j N_i f_d \left(\sum_{k=1}^{n_{el}} \rho_k(t) N_k, \sum_{k=1}^{n_{el}} c_k(t) N_k \right) - \delta_1 N_j N_i f_e \left(\sum_{k=1}^{n_{el}} c_k(t) N_k \right) d\Omega \right) \rho_i(t)$$

- **Transport equation**:

$$\int_\Omega \left(N_j(x) \partial_t \sum_{i=1}^{n_{el}} c_i(t) N_i(x) + N_j(x) \partial_x \left(\sum_{i=1}^{n_{el}} c_i(t) N_i(x) \right) \sum_{i=1}^{n_{el}} v_i(t) N_i(x) \right) d\Omega =$$

$$\int_\Omega \left(\delta_3 N_j(x) f_p(x) - \frac{1}{2} N_j(x) f_d \left(\sum_{i=1}^{n_{el}} \rho_i(t) N_i(x), \sum_{i=1}^{n_{el}} c_i(t) N_i(x) \right) \sum_{i=1}^{n_{el}} c_i(t) N_i(x) \right) d\Omega -$$

$$\int_\Omega \left(\delta_4 N_j(x) \sum_{i=1}^{n_{el}} c_i(t) N_i(x) \right) d\Omega$$

$$\sum_{i=1}^{n_{el}} \int_\Omega N_j N_i c_i'(t) + N_j N_i' \left(\sum_{k=1}^{n_{el}} v_k(t) N_k(x) \right) c_i(t) d\Omega =$$

$$\sum_{i=1}^{n_{el}} \left(\int_\Omega \delta_3 N_j f_p(x) - \frac{1}{2} N_j N_i f_d \left(\sum_{i=1}^{n_{el}} \rho_i(t) N_i(x), \sum_{i=1}^{n_{el}} c_i(t) N_i(x) \right) - \delta_4 N_j N_i d\Omega \right) c_i(t)$$

- **Momentum balance**:

$$\int_\Omega \left(\partial_x N_j(x) \left(\kappa f_k \left(\sum_{i=1}^{n_{el}} c_i(t) N_i(x) \right) \left[1 - \left(\frac{\sum_{i=1}^{n_{el}} \rho_i(t) N_i(x)}{f_\rho(\sum_{i=1}^{n_{el}} c_i(t) N_i(x))} \right)^{3/2} \right] \right) \right) d\Omega +$$

$$\int_\Omega \left(2 \partial_x N_j(x) \partial_x \sum_{i=1}^{n_{el}} v_i(t) N_i(x) + \ell_h N_j(x) \sum_{i=1}^{n_{el}} v_i(t) N_i(x) \right) d\Omega = 0$$

$$- \int_\Omega N_j' \left(\kappa f_k \left(\sum_{i=1}^{n_{el}} c_i(t) N_i(x) \right) \left[1 - \left(\frac{\sum_{i=1}^{n_{el}} \rho_i(t) N_i(x)}{f_\rho(\sum_{i=1}^{n_{el}} c_i(t) N_i(x))} \right)^{3/2} \right] \right) d\Omega =$$

$$\sum_{i=1}^{n_{el}} \left(\int_\Omega \left(2 N_j' N_i' + \ell_h N_j N_i \right) d\Omega \right) v_i(t)$$

3.3 Time discretization

Our model is system of partial differential equations. It has a peculiarity, though: there are two differential variables, ρ and c, the time derivatives of which appear in the conservation and transport equations. Initial conditions have to be provided for these two variables. On the other hand, time derivatives of the velocity does not appear in any of the equations. Hence, initial conditions are not required for it, since the initial velocity can be computed from the initial concentration and density using the momentum balance equation.

In general time evolution can be a very difficult issue to tackle. The simplest way to solve it is considering an **staggered scheme**. That is, each equation is evolved independently from the other two, where the variables which are not derived in time are considered at the previous time step. The algorithm is the following:

1. Compute v^{n+1} using the values of ρ^n and c^n using the momentum balance equation.
2. Compute ρ^{n+1} using c^n and v^{n+1} form the conservation equation.
3. Compute c^{n+1} using ρ^{n+1} and v^{n+1} from the transport equation.
4. Iterate until convergence.

As for the time discretization, we use a hybrid formulation. That is, the non-linear terms are considered at iteration n and the linear terms are considered at time $n+1$. This formulation has the advantage of being easy to implement, since the final expression is linear, but it is more stable than the fully explicit formulation. where very small step sizes are required. The final expressions for each equation are:

- Conservation equation:

$$\sum_{i=1}^{n_{el}} \int_\Omega \left(N_j N_i \frac{\rho_i^{n+1} - \rho_i^n}{\Delta t} - N_j' N_i \left(\sum_{k=1}^{n_{el}} v_k^n N_k \right) \rho_i^{n+1} \right) d\Omega$$

$$= \sum_{i=1}^{n_{el}} \left(\int_\Omega \left(N_j N_i f_d \left(\sum_{k=1}^{n_{el}} \rho_k^n N_k, \sum_{k=1}^{n_{el}} c_k^n N_k \right) - \delta_1 N_j N_i f_e \left(\sum_{k=1}^{n_{el}} c_k^n N_k \right) \right) d\Omega \right) \rho_i^{n+1}$$

$$\sum_{i=1}^{n_{el}} \left(\int_\Omega \left(N_j N_i - \Delta t \left(N_j' N_i v^{n+1} + N_j N_i f_d \left(\rho^n, c^n \right) - \delta_1 N_j N_i f_e \left(c^n \right) \right) \right) d\Omega \right) \rho_i^{n+1}$$

$$= \sum_{i=1}^{n_{el}} \left(\int_\Omega N_j N_i d\Omega \right) \rho_i^n$$

- Transport equation:

$$\sum_{i=1}^{n_{el}} \int_\Omega \left(N_j N_i \frac{c_i^{n+1} - c_i^n}{\Delta t} + N_j N_i' v^{n+1} c_i^{n+1} \right) d\Omega$$

$$= \sum_{i=1}^{n_{el}} \int_\Omega \left(\delta_3 N_j f_p(x) - \left(\frac{1}{2} N_j N_i f_d \left(\rho^{n+1}, c^n \right) + \delta_4 N_j N_i \right) c_i^{n+1} \right) d\Omega$$

$$\sum_{i=1}^{n_{el}} \left(\int_\Omega \left(N_j N_i + \Delta t \left(N_j N_i' v^{n+1} + \frac{1}{2} N_j N_i f_d \left(\rho^{n+1}, c^n \right) + \delta_4 N_j N_i \right) \right) d\Omega \right) c_i^{n+1}$$

$$= \sum_{i=1}^{n_{el}} \int_\Omega \left(\Delta t \delta_3 N_j f_p(x) + N_j N_i c_i^n \right) d\Omega$$

- Momentum balance:

$$\sum_{i=1}^{n_{el}} \left(\int_\Omega \left(2N_j' N_i' + \ell_h N_j N_i \right) d\Omega \right) v_i^{n+1} = - \int_\Omega N_j' \left(\kappa f_k \left(c^n \right) \left[1 - \left(\frac{\rho^n}{f_\rho(c^n)} \right)^{3/2} \right] \right) d\Omega$$

As for the value of the time step, a constant value which is small enough to assure convergence is considered ($h = 10^{-3}$). Some improvements can be considered to solve the system in a more efficient way (see appendix B), but we will not discuss them in detail.

3.4 Parameters

Once we have the discretized model ready to be implemented, the last step consists on determining the values of the adimensional parameters. In order to do so, we adjust these values to the real physical values of the problem. Some of these values can be obtained experimentally from measurements in intestinal organoids [16]. Most of them, however, are simply average values, since they can vary depending on a large amount of factors. The following table shows the values for each of the parameters that can be measured experimentally:

Parameter	Description	Value
L	Length of the domain (mean distance between crypts)	$100\mu m$
l_{gauss}	Width of the Gaussian (radius of the crypts)	$10\mu m$
$\bar{k_d}$	Maximum division rate	$10^{-2}h^{-1}$
$\bar{k_e}$	Maximum extrusion rate	$10^{-2}h^{-1}$
$\bar{k_p}$	Maximum rate of Wnt generation	$0.5 \cdot 10^{-2}h^{-1}$
ρ_0(i)	Mean density of cells inside the crypts	$5.25 \cdot 10^{-2}\mu m^{-2}$
ρ_0(ii)	Mean density of cells inside the villus	$2.5 \cdot 10^{-2}\mu m^{-2}$
$\bar{k}(i)$	Elastic constant inside the crypt	$2.7mN \cdot m^{-1}$
$\bar{k}(ii)$	Elastic constant inside the villus	$1.8mN \cdot m^{-1}$
μ	Viscosity coefficient	$1kPa \cdot \mu m^{-1} \cdot s$
η	Friction coefficient	$10^3 kPa \cdot \mu m \cdot s$

Table 1: Experimental values of the parameters.

Note that we have two values for ρ_0 and k, corresponding to the values inside the crypt and at the villus. We will use the values inside the crypt to adimensionalize the equations. Since these are simply average values obtained experimentally, they only provide information on the order of magnitude of the parameters. What's more, there are some parameters which are unfeasible to be computed in practice, like $\bar{k_p}$ and $\bar{k_n}$, so we will have to determine their value by fitting the results from simulations.

With these values we can compute some adimensional parameters:

- $\delta_1 = \frac{\bar{k_e}}{\bar{k_d}} = \frac{10^{-2}h^{-1}}{10^{-2}h^{-1}} = 1.$
- $\ell = \frac{l_{gauss}}{L} = \frac{10\mu m}{100\mu m} = 0.1.$

- $l_h = \sqrt{\frac{\mu}{\eta}} = \sqrt{\frac{10^3 kPa \cdot \mu m \cdot s}{1 kPa \cdot \mu m^{-1} \cdot s}} = 31 \mu m.$
- $\ell_h = \left(\frac{L}{l_h}\right)^2 = \left(\frac{100 \mu m}{31 \mu m}\right)^2 = 10.$
- $\kappa = \frac{\bar{k}}{2\mu \bar{k_d}} = \frac{2.7 mN \cdot m^{-1}}{2 \cdot 10^3 kPa \cdot \mu m \cdot s \cdot 10^{-2} h^{-1}} = 10^3.$

4. Results

4.1 Convergence analysis

Once we have defined our model we are interested in studying the convergence of the system, and in the case we have convergence what kind of steady states we can have. From a qualitative point of view, we may expect several situations. The desired one is a system divided in two regions, the villus and the crypt, such that the density in the crypt is higher than the density in the villus. A second situation corresponds to the total extinction of both the stem cells and enterocytes. That is, that ρ converges to zero (although c may not converge to zero, since we assume that the paneth cells are fixed and they would still segregate Wnt). This situation may take place when extrusions are too fast with respect to divisions, or when the Wnt is produced at a very small rate compared to cell division. The last possible situation is that the concentration diverges. This may happen whenever extrusions occur at a rate which is too slow or when Wnt is generated at a very high rate.

From a numerical point of view, we found that the parameters which regulate the behaviour of the system are δ_1 and δ_3, which are the rates between extrusions and divisions, and the rate between Wnt generation by the Paneth cells and cell division, respectively. We observe three behaviours:

- **Convergence to zero**: We found that, whenever δ_1 is very large (of the order of 2 or higher) or when δ_3 is too small (of the order of 0.5 or smaller), the cell density converges to 0. This situation corresponds to the extrusion of all the cells, thus provoking the disappearance of the organoid. This can be seen in Fig. 2 (a) for a set of parameters $\delta_1 = 2$, $\delta_2 = 1$, $\delta_3 = 0.5$, $\delta_4 = 1$, $\epsilon = 0.02$, $\ell = 0.1$, $l_h = 10$ and $\kappa = 10^3$.
- **Convergence to a non-zero state**: When δ_1 and δ_3 take intermediate values (δ_1 around 1 and δ_3 between 1 and 4) the system converges to a non-trivial state, in which we observe two distinct regions correpsonding to the villus and the crypt. This can be seen in Fig. 2 (b) for a set of parameters $\delta_1 = 0.8$, $\delta_2 = 1$, $\delta_3 = 3$, $\delta_4 = 1$, $\epsilon = 0.02$, $\ell = 0.1$, $l_h = 10$ and $\kappa = 10^3$.
- **Divergence**: We found that, whenever δ_1 is very small (of the order of 0.5 or less) or when δ_3 is too large (of the order of 4 or greater), the system diverges. We can observe that because the system reaches a state where oscillations start to appear, and the system does not converge. This can be seen in Fig. 2 (c) for a set of parameters $\delta_1 = 0.4$, $\delta_2 = 1$, $\delta_3 = 5$, $\delta_4 = 1$, $\epsilon = 0.02$, $\ell = 0.1$, $l_h = 10$ and $\kappa = 10^3$.

From a biological point of view we are interested in the second case, the one where the system converges to a non-zero state. The first case corresponds to the extinction of the organoid, and the third one has no physical sense, since it implies that the density would increase up to infinity. Hence, we will consider intermediate values for both variables in order to have the two regions we are interested in, the villus and

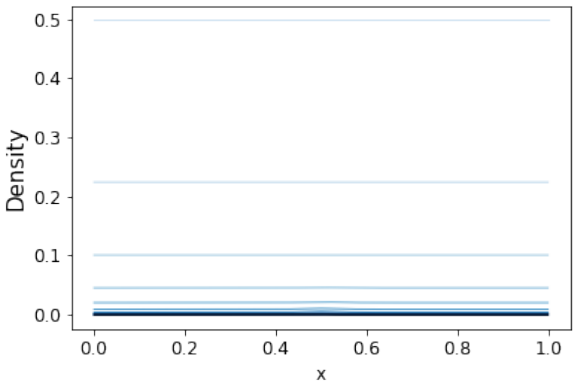

(a) Convergence to zero.

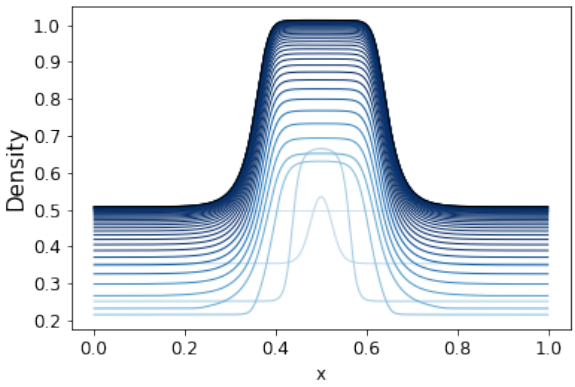

(b) Convergence to a non-zero state.

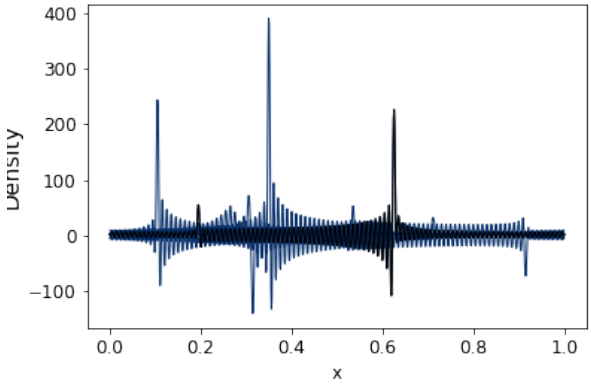

(c) Divergence.

Figure 2: Evolution of the cell density ρ in the three different behaviours of the system.

the crypt. The following subsection focuses on the description of this system, and characterizes the two regions.

4.2 Homeostatic steady state

Our first goal is to determine the **homeostatic steady state**, which mimics that observed in intestinal organoids [1] and is highly out-of-equilibrium and characterized by steady but heterogeneous density and cell identity distributions, and at the same time by a continuous motion, division and extrusion of cells. In particular, we want to observe a system divided in two regions, which correspond to the crypt and the villus. These two regions are characterized by the following behaviour:

- **Crypt**: The cells are highly packed, so the density is very high inside the crypt. The width of the crypt is proportional to the gaussian width (it should occupy around 20% of the domain length). This is the region where Paneth cells lie, so the concentration of Wnt is also large inside the crypt. This is also the place where divisions take place, but extrusions do not occur inside the crypt. As

for the velocity field, we expect it to expel the cells outside the crypt, so it should point towards the villus.

- **Villus**: The cell density at the villus is lower than in the crypt (from experimental values we expect it to be around half of the density inside the crypt, see 3.4). We do not have Paneth cells inside the villus, so the Wnt concentration will be small (the concentration will decrease as we go further from the crypt). Cell divisions do not take place at the villus. Instead, extrusions take place there. As for the velocity field, we expect it to point towards the inside of the villus as well.

Fig. 3 corresponds to the equilibrium state obtained for the following set of adimensional parameters: $\delta_1 = 0.8$, $\delta_2 = 1$, $\delta_3 = 3$, $\delta_4 = 1$, $\epsilon = 0.02$, $\ell = 0.1$, $I_h = 10$ and $\kappa = 10^3$. All the variables in the figures are in adimensional form. That is, since we adimensionalize ρ by ρ_0 inside the crypt, we precisely obtain the mean values of the cell density both inside and outside of the crypt. Moreover, if we consider that the crypt is the region where $c > 1$, then the width of the crypt is approximately 20% of the domain size, as expected. As for the division and extrusion rates they both behave as expected: division only happens inside the crypt and extrusion outside of the crypt. The velocity field also point towards the villus, being maximum at the edge of the crypt and minimum at the center of the crypt and the center of the villus.

Observe that we have two stagnation points. That is, two points where the velocity is zero. These points are usually delicate to treat, since they can give rise to numerical errors. In this case we observe that the concentration has a critical point precisely at the stagnation point at $x = 0$ (meaning that c presents a peak at this point, where c is not differentiable with respect to x).

It is also interesting to study the transient that the system experiences until it reaches the homeostatic equilibrium state, and interpret it in physical terms. This can be seen in Fig. 4. Observe that c is initially 0 everywhere, and it starts to increase around $x = 0.5$, where the paneth cells lie. The Wnt then travels to the exterior of the crypt until it occupies the whole domain, and the maximum Wnt concentration reaches a maximum value, since for very high c divisions are very frequent, so there is an equilibrium between the generation of Wnt and the decrease of its concentration due to cell divisions. As for the cell density, it initially decreases, because $c = 0$ everywhere at $t = 0$. However, once the concentration of Wnt is high enough at the crypt, the cell density starts to increase in the crypt as well, and it reaches an equilibrium value both inside and outside the crypt. The dynamics of v are conditioned to the dynamics of c and ρ, since there are no time derivatives of this variable in the model, so its time evolution is not as interesting as for the other two variables. However, it is interesting to notice that at the beginning v points towards the crypt. However, after a very short period of time, this effect is reverted and v presents a maximum at the transition region between the crypt and the villus, pointing towards the villus.

The main result we can conclude from this analysis is the spontaneous organization into this steady-state where the system does not change by continuously changing. This is precisely the homeostatic behaviour the intestinal organoids present.

4.3 Initial conditions

We have stated that the previous state is an homeostatic equilibrium state. That is, the system converges to this state after a transition. However, this behaviour may depend on the initial state. We need to verify whether the system converges to this state regardless of the initial condition of the system (assuming reasonable initial conditions, that is, conditions which make physical sense). As we explained in 3.3, we only need to impose initial conditions for ρ and c, since v is computed directly from ρ and c through the momentum balance equation. Several examples are considered:

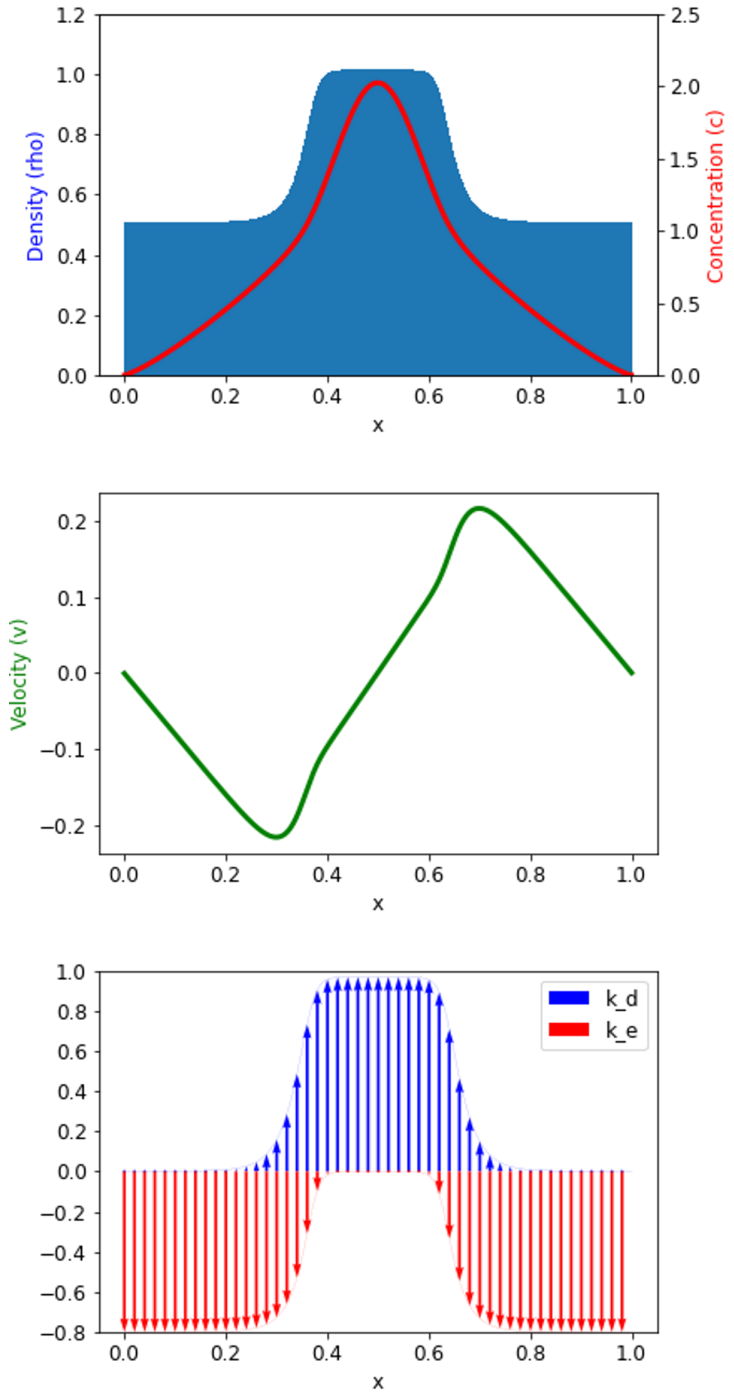

Figure 3: Homeostatic equilibrium state. (Top) Density and Wnt concentration at the equilibrium state. (Middle) Velocity field at the equilibrium state. Positive sign of v to the right. (Bottom) Division (blue) and extrusion (red) rates at the equilibrium state.

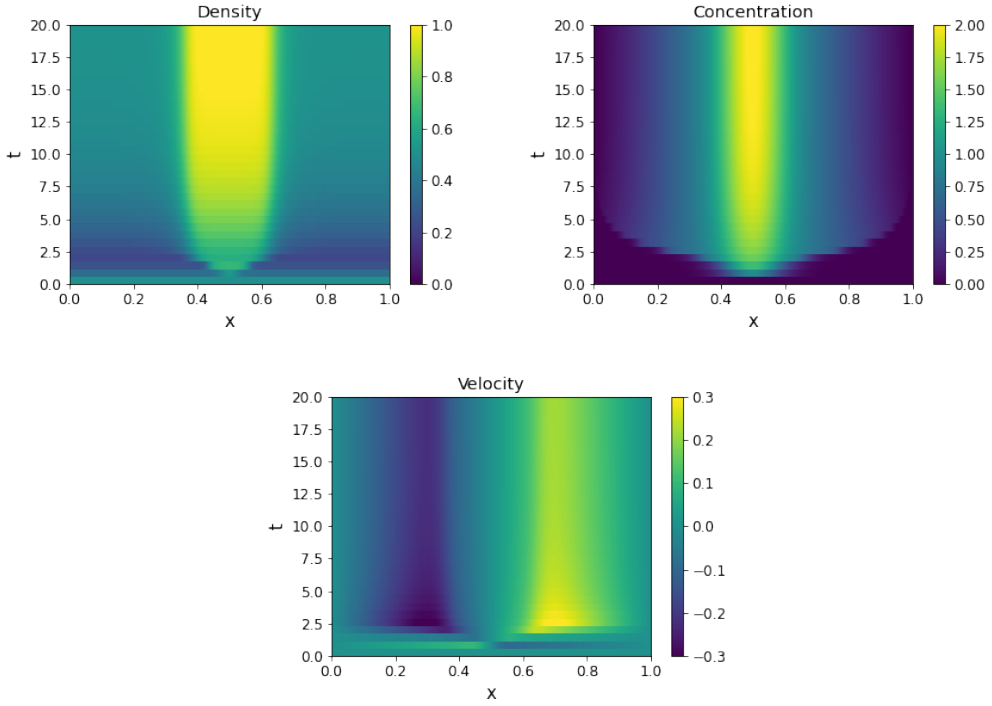

Figure 4: Time evolution of each of the variables in the system until the system it reaches the homeostatic equilibrium state.

- **Null initial conditions**: As a first test, we can check what happens if we consider null initial conditions for ρ and c. In this case, we are on an unstable equilibrium point. That is, we expect the density to remain zero for all times, since if we do not have any cells they cannot divide and grow, nor extrude (this can also be checked in the equations of the model). Fig. 5 (a) shows that this is indeed the result we observe. This result just serves us to ensure that our model is consistent (that is, that from null initial conditions we recover null density).

- **Null Wnt concentration**: The second option consists on assuming that the initial density is constant and equal to 0.5 (which is the mean density at the villus), and that the Wnt concentration is initially null. This example corresponds to the spontaneous creation of the crypt at the center of the domain when Paneth cells generate Wnt. Fig. 5 (b) shows the time evolution of this system. Observe that, since c is initially null, the density tends to decrease everywhere, since there are only extrusions. However, as c starts to increase due to the Wnt generation by the Paneth cells, the density starts to increase until it reaches the equilibrium state.

- **Initial Wnt concentration**: A third example corresponds to considering that the Wnt concentration is initially not zero ($c = 1$ everywhere), with constant initial density $\rho = 0.5$. This case corresponds to a situation where there is already some Wnt concentration in the system, but the crypt has not formed yet. Fig. 5 (c) shows the time evolution of this system. The general behaviour is very similar to the one observed for initial null Wnt concentration, although now the density does not decrease as fast as before since c is initially not null.

- **Initial sinusoidal density**: As a final example, we can consider a non-constant initial density. For

instance, we can consider that the cell density is sinusoidal (and null Wnt concentration), and see whether even in that case we converge to the same equilibrium state. Fig. 5 (d) shows the time evolution of a system with sinusoidal initial condition. We observe that it ends up converging to the same equilibrium state.

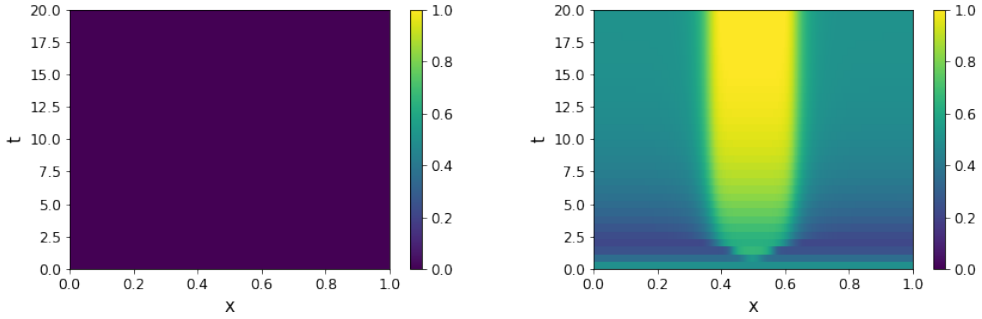

(a) Initial null cell density and null Wnt concentration.

(b) Initial constant cell density $\rho = 0.5$ and null Wnt concentration.

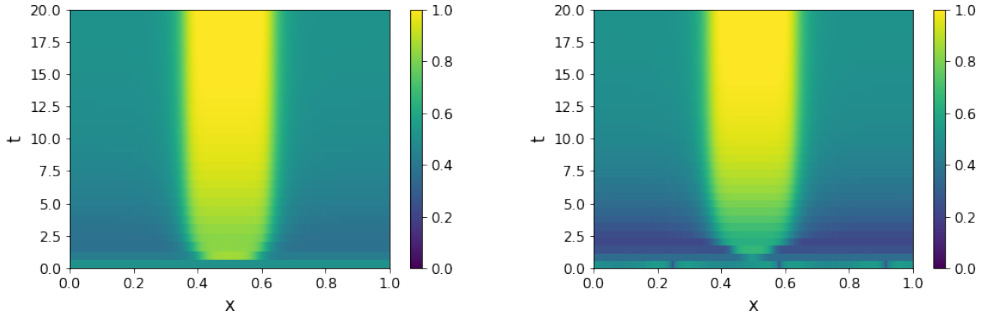

(c) Initial constant cell density $\rho = 0.5$ and constant Wnt concentration $c = 1$.

(d) Initial sinusoidal cell density and null Wnt concentration.

Figure 5: Time evolution of the system under different initial conditions, both for ρ and c.

These results show the robustness of the self-organized homeostatic steady state, since it does not depend on the initial conditions. From now on, unless the opposite is said, we will consider the initial state to be $\rho = 0.5$ everywhere in the domain and $c = 0$ in the whole domain as well. This corresponds to the most realistic case, in which the crypt forms spontaneously due to the segregation of Wnt by the paneth cells in a region where initially the cell density is that of the villus.

4.4 Effect of the parameters

The second aspect to study in our model is which is the effect of each of the parameters. In particular, we are interested in determining the range of admissible values for each of them, studying what happens in the limit case in which each parameter tends to zero or to infinity and give a physical interpretation of their effect. Observe that the parameters which have a physical importance are the adimensional parameters, since they are independent with each other. Hence, we will vary them with respect to their value in the homeostatic equilibrium state to see how they affect the solution.

- **Size of the crypt**

  First of all, we can study what is the effect of changing ℓ. This quantity is the ratio between the gaussian width and the size of the domain, so it is directly related to the size of the crypt. In particular, values $\ell > 1$ do not make physical sense.

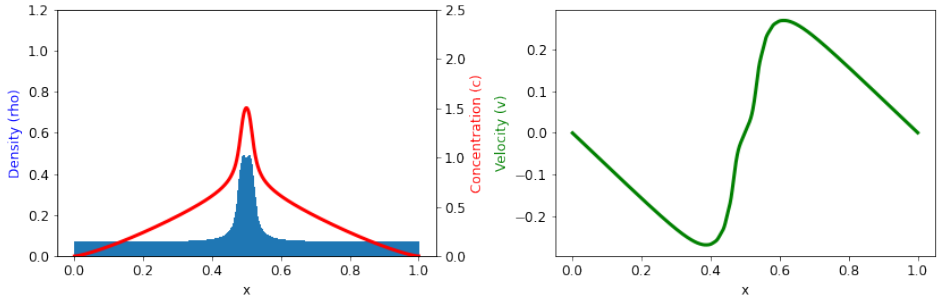

(a) $\ell = 0.02$, $l_{gauss} = \frac{L}{50}$.

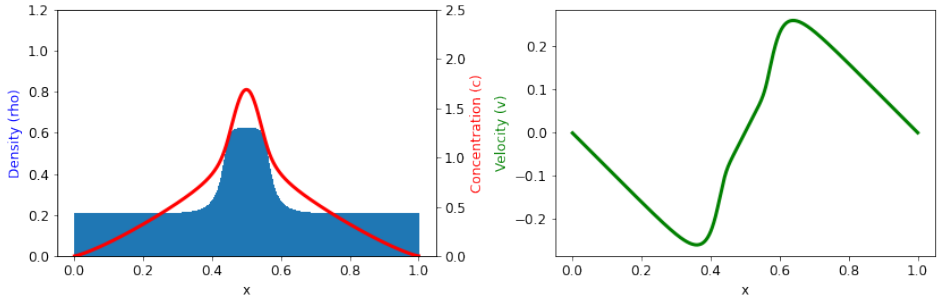

(c) $\ell = 0.05$, $l_{gauss} = \frac{L}{20}$.

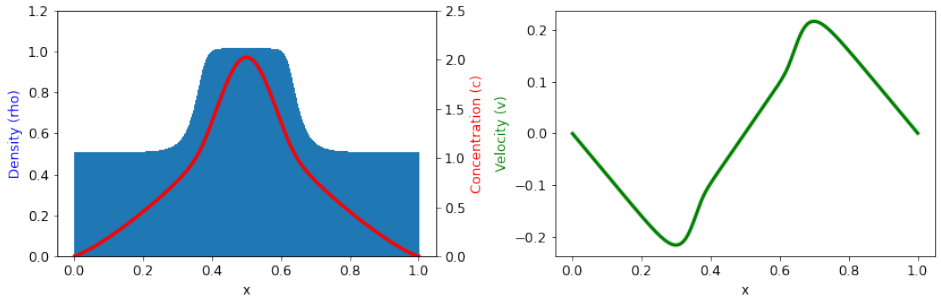

(d) $\ell = 0.1$, $l_{gauss} = \frac{L}{10}$.

Figure 6: Equilibrium state under different crypt widths (different values of ℓ).

Fig. 6 shows the equilibrium state obtained for several values of ℓ. As expected, small values of ℓ correspond to narrow crypts, and large values of ℓ correspond to wide crypts (all of this with respect to the mean distance between neighbour crypts). It is interesting to notice that for small crypt sizes the density at the villus decreases. This is consistent with the fact that enterocytes are generated at the crypts and advected to the villus. Hence, if the villus is large in comparison with the crypt size the cells have to occupy a very large size and the density decreases. The size of the crypt is precisely the one required to have the densities we require both inside the crypt and outside the crypt. Observe

that, for very small gaussian widths (fig. 6 (a)), some oscillations appear in the density at the crypt. This means that we would require more elements to model this situation correctly, although the general behaviour w are studying would be the same.

- **Hydrodynamic length**

  Another parameter we can play with is the hydrodynamic length. This magnitude is regulated by ℓ_h, which is the square of the ratio between the size of the domain and the hydrodynamic length. The hydrodynamic length is related to the distance at which one part of the domain interacts with another one. That is, if the hydrodynamic length is very high, what happens in a region affects the whole domain. On the contrary, small hydrodynamic lengths imply that each region of the domain is independent from the neighbour regions.

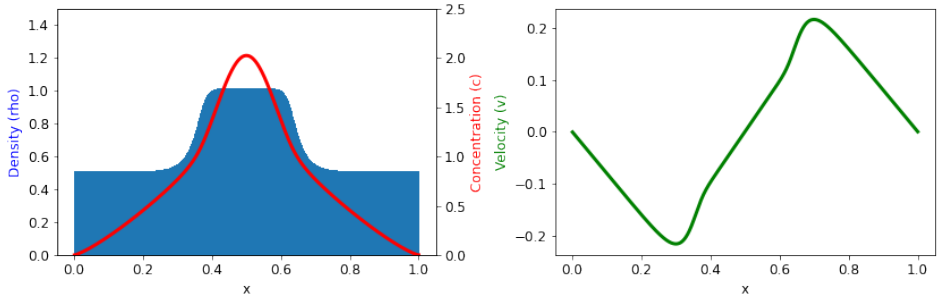

(a) $\ell_h = 10$, $l_h = \frac{L}{3.162}$.

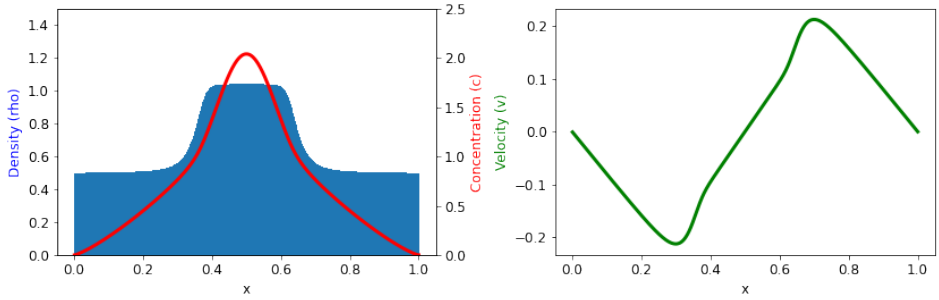

(b) $\ell_h = 1000$, $l_h = \frac{L}{31.62}$.

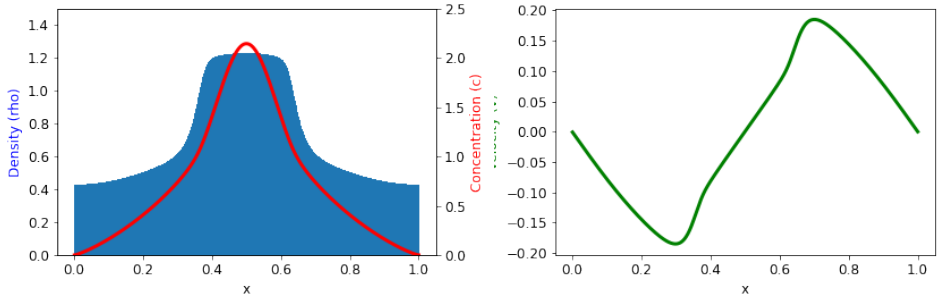

(c) $\ell_h = 10000$, $l_h = \frac{L}{100}$.

Figure 7: Equilibrium state under different hydrodynamic lengths (different values of ℓ_h).

Fig. 7 shows the equilibrium state for several values of the hydrodynamic length. We start to observe differences in the solution for $\ell_h = 1000$, which corresponds to a hydrodynamic length which is 3.1% the domain size. For large hydrodynamic lengths this distance is too large with respect to the domain size and in practice this term becomes irrelevant in the momentum balance equation. However, for small hydrodynamic lengths, the effect we observe is that the density increases at the crypt. This happens because the term $\ell_h v$ corresponds to a friction force, so when friction is large (that is, ℓ_h is large) the cells are less likely to escape the crypt, so the density increases. We also found that if we increase ℓ_h too much the program diverges, a result in agreement with the same idea. That is, if the friction is too large the velocity decreases a lot and cells are not able to move, resulting in an increase in density at the crypt.

- **Stiffness**

  The magnitude of the elastic stress is regulated by the stiffness parameter κ. This term is related to the tendency that the system has to go back to the equilibrium state, which in this case is given by $\rho_0(c)$. That is, when the elastic stress is large, the density is more likely to have a value close to $\rho_0(c)$ at every point.

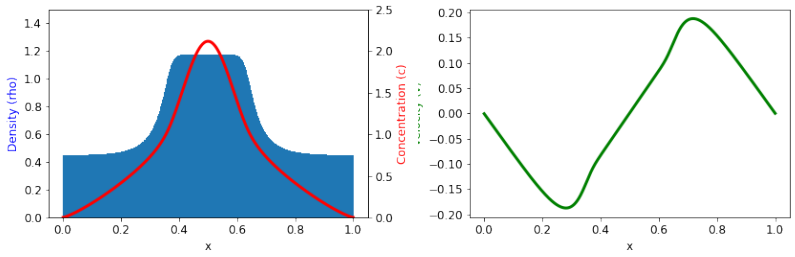

(a) $\kappa = 10$.

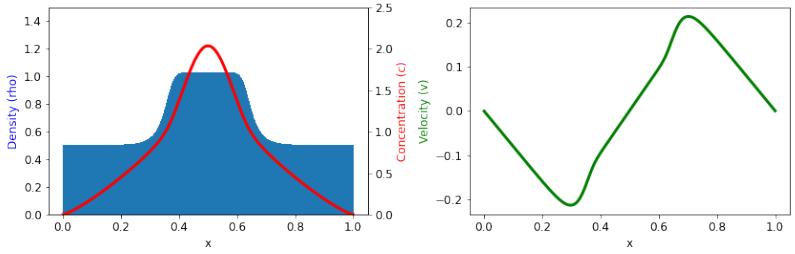

(b) $\kappa = 100$.

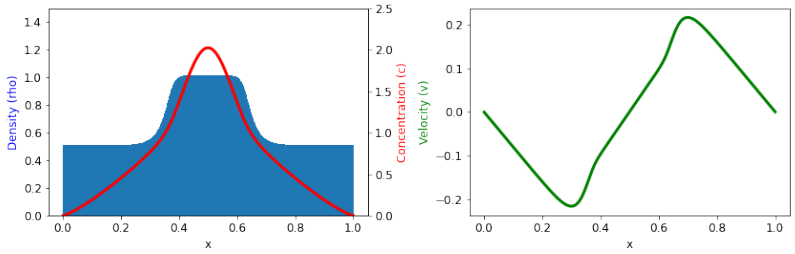

(c) $\kappa = 1000$.

Figure 8: Equilibrium state under different elasticity constants (different values of κ).

Fig. 8 shows the equilibrium state for several values of κ. Observe that, when κ has a high value, the density both inside and outside the crypt is very close to the equilibrium value (1 inside the crypt and 0.5 at the villus). On the contrary, if the elastic stress is small, the density inside the crypt increases, while the density at the villus decreases. This can be understood in a similar way as the effect of changing ℓ_h: if we decrease the effect of the elastic stress, the viscous and friction terms become more relevant, and the overall effect is that cells are less likely to leave the crypt, so the density inside the crypt increases, while the density at the villus decreases.

As with the hydrodynamic length, there is a point at which increasing κ has no effect because the elastic stress is already the predominant term in the momentum equation. What's more, for very big elastic stresses the time step has to be very small, since the velocity increases as well, so we need to perform more iterations to reach convergence.

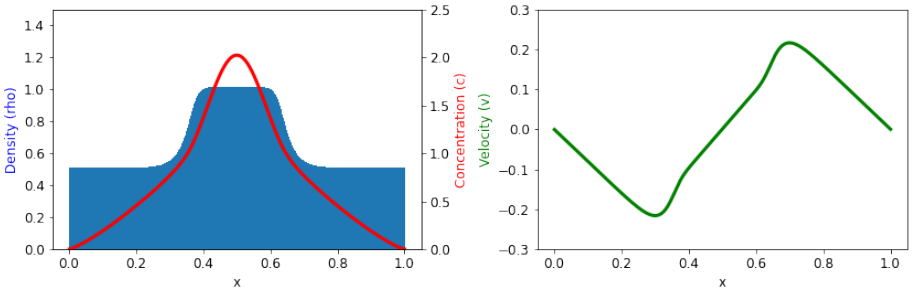

(a) $\delta_4 = 1$.

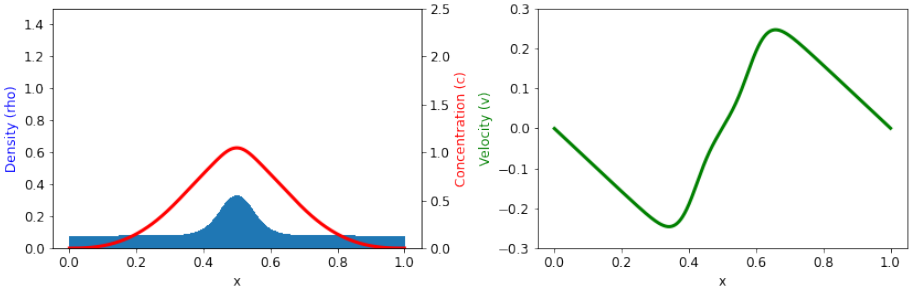

(b) $\delta_4 = 2$.

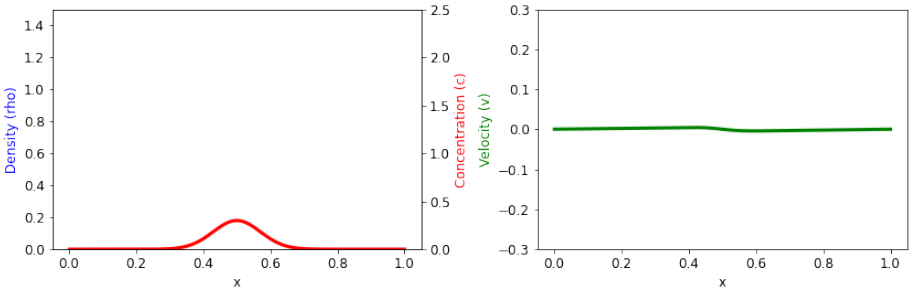

(c) $\delta_4 = 10$.

Figure 9: Equilibrium state under different degradation parameters (different values of δ_4).

- **Degradation parameter**

  Another important parameter is the degradation parameter (δ_4 after adimensionalization). Unlike the previous parameters, the degradation parameter is very hard to measure experimentally, so we have no criteria to decide its value other than using qualitative arguments and matching the results from simulations to the experimental results. This parameter regulates the speed at which Wnt degradates due to a large amount of factors, in contrast to the reduction of c due to cell divisions. We expect this value to have a large impact on the equilibrium state. On one hand, if the degradation parameter is large, Wnt degradates at a very high speed. c will be small in all the domain and there will be a lot of extrusions (even inside the crypt), so the system may end up extinguishing. On the other hand, if δ_4 is small, the only way to reduce the Wnt concentration is by means of cell division, so the Wnt concentration will be much higher and its dynamic will only be regulated by cell division and cell extrusion.

  Fig. 9 shows the equilibrium state for several values of the degradation parameter. As expected, for large values of δ_4 the cell density goes to zero. If δ_4 is too small numerical oscillations appear near $x = 0$ (see 4.5).

- **Ratio between thresholds**

  There is another parameter which we cannot measure experimentally: the ratio between thresholds for cell division and cell extrusion. Our assumption is that, for large Wnt concentrations, the cells divide so as to reduce this concentration, and once the cells have divided extrusion begins. However, there is a range of values of c for which division has ended but extrusion has not begun yet. This range of values is regulated by δ_2, and we expect it to be smaller than 1 ($\delta_2 = \frac{c_e}{c_d} < 1_e < c_d$, so that extrusion begins after division ends, and not before).

  Fig. 10 shows the cell density and Wnt concentration for several values of δ_2, as well as the division and extrusion rates, which are the most interesting magnitudes for this case. We can observe that, when δ_2 is small, there is no overlapping in the regions where extrusions and divisions take place, so the two regions in space are completely differentiated one from the other. This results in an increase of the cell density, since extrusions are less common. It is interesting to notice that, although the value of c is higher at the crypt for small values of δ_2, the division rate is smaller. This happens because the cell density is also larger, and the division rate also depends on ρ (for high densities, cells are less likely to divide because they are more packed and the division rate decreases). On the contrary, for large δ_2, extrusions takes place everywhere in the domain (a non-realistic situation), and the division rate is also larger because, although the Wnt concentration is smaller, the cell density is smaller as well.

- ϵ

  There is another parameter which is related to the division rate, ϵ. The term $\frac{\epsilon}{\rho+\epsilon}$ decays to zero when $\rho \to \infty$, and the smaller ϵ the fastest this decay is. Hence, ϵ is related to the speed of the decay of the division rate with respect to the cell density.

  Fig. 11 shows the equilibrium state for several values of ϵ. Observe that, for small values of ϵ, the transition region between the crypt and the villus becomes steeper, and the density is smaller than for large ϵ. From a mathematical point of view, this happens because the division rate decays very fast when the density is greater than zero, and the consequence is that the cell density decreases. Moreover, the velocity of advection of the cells is also smaller, so the cells are less likely to leave the crypt. This provokes that the cell density is also smaller at the villus, tending to zero in the limit case where ϵ is very small.

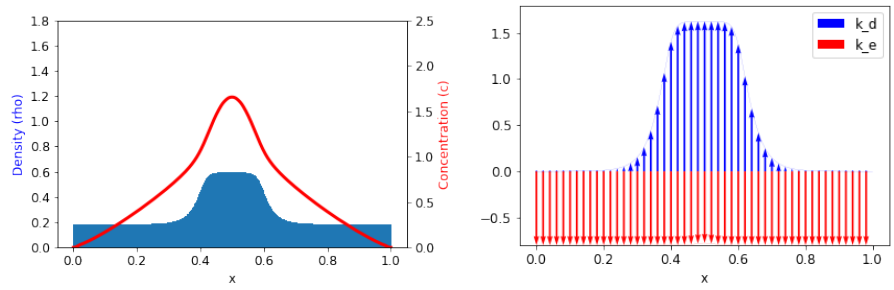

(a) $\delta_2 = 2$.

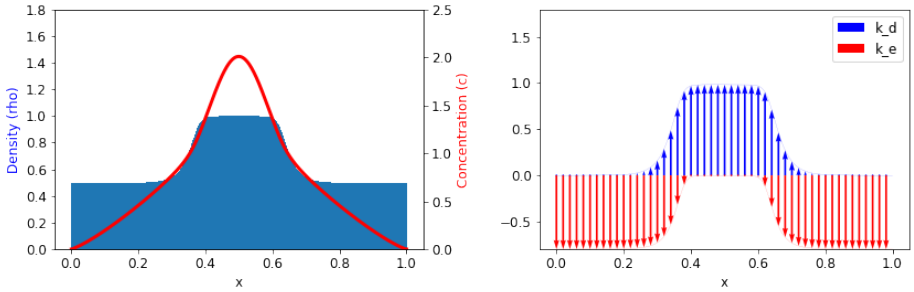

(b) $\delta_2 = 1$.

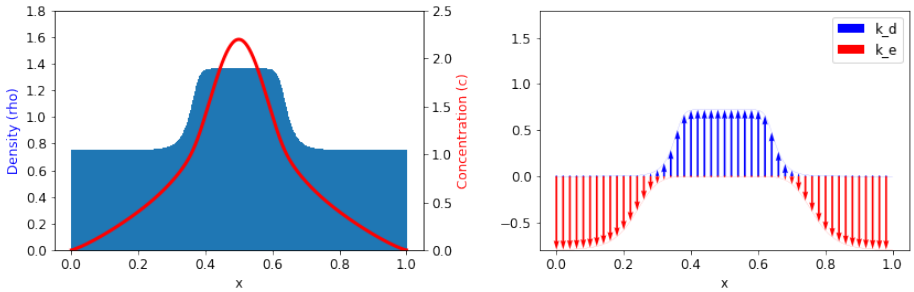

(c) $\delta_2 = 0.5$.

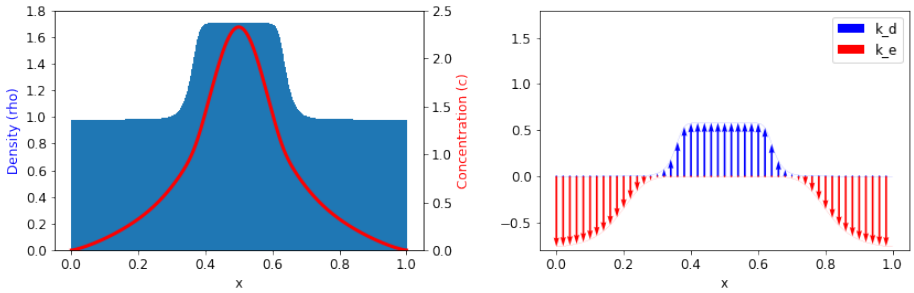

(d) $\delta_2 = 0.3$.

Figure 10: Equilibrium state under different values of the ratio between thresholds (different values of δ_2).

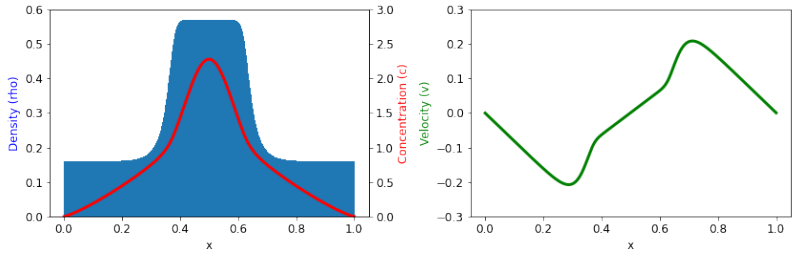

(a) $\epsilon = 1$.

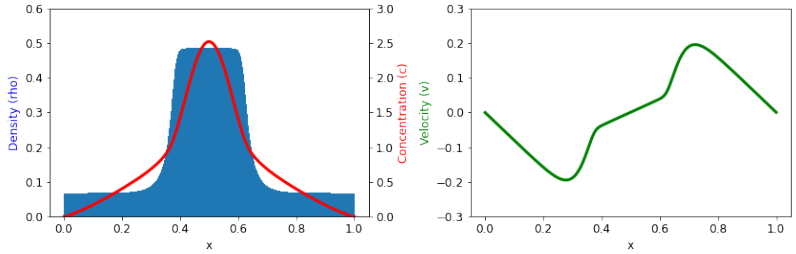

(b) $\epsilon = 0.3$.

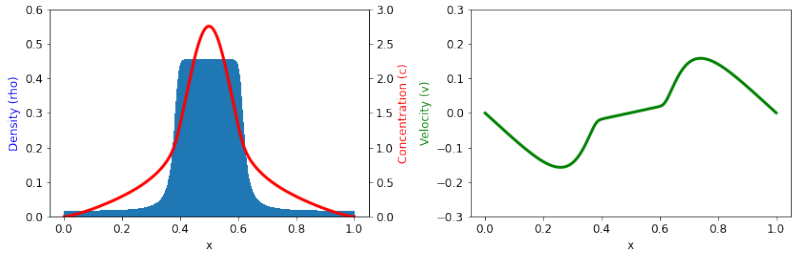

(c) $\epsilon = 0.1$.

Figure 11: Equilibrium state under different values of ϵ.

There are two adimensional parameters, δ_1 and δ_3, which have not been discussed in this section. These parameters are related, as they both have a huge impact on the behaviour of the system. A more exhaustive discussion about their behaviour is done in 4.6.

4.5 Importance of degradation

Degradation of Wnt plays a key role in the dynamics of the system, since it is the only way to eliminate Wnt (cell divisions only decrease its concentration, but the Wnt is not destroyed). Numerically, what is observed is that δ_4 acts as a stabilization parameter. That is, if it goes to zero numerical oscillations start to appear. This can be explained in terms of the system of equations of the model, studying the equilibrium points of such system.

Let's consider the transport equation for c:

$$\partial_{\bar{t}}\bar{c} + \partial_{\bar{x}}\bar{c}\bar{\mathbf{v}} = \delta_3 f_p(x) - \frac{1}{2} f_d(\bar{\rho}, \bar{c})\bar{c} - \delta_4 \bar{c} \tag{32}$$

As we have seen in all the simulations, the system presents two stagnation points: $x = 0$ and $x = 0.5$. These two points are equilibrium points, since the velocity is zero in both of them. The reason why the velocity is zero in these points is a symmetry argument: the system presents symmetry with respect to the center of the gaussian $x = 0.5$, so these point must have $v = 0$. Moreover, since the domain is periodic, the point which lies in the middle of two consecutive gaussians ($x = 0$) is also a stagnation point. Hence, if we evaluate the trasport equation in equilibrium ($\partial_{\bar{t}}\bar{c} = 0$) in any of these points we get:

$$0 = \delta_3 f_p(x) - \frac{1}{2} f_d(\bar{\rho}, \bar{c})\bar{c} - \delta_4 \bar{c}$$

and since $f_p(0) = 0$, this expression evaluated at $x = 0$ yields:

$$0 = -f_d(\bar{\rho}, \bar{c})\bar{c} - \delta_4 \bar{c}$$

This equation has only one solution, which is $c = 0$, since both $f_d(\bar{\rho}, \bar{c}) > 0$ and $\delta_4 > 0$. Hence, in equilibrium, the concentration at $x = 0$ is always zero.

If there is no degradation, $\delta_4 = 0$, so Wnt never reaches the point $x = 0$. However, Wnt is not eliminated from the system (the concentration is only reduced by means of cell divisions), and it is advected towards the villus. The effect is then the creation of a shock wave towards $x = 0$, and we end up having a boundary layer next to $x = 0$ where the Wnt concentration increases drastically in a very small region. This can be observed in Fig. 12. Moreover, this shock wave presents numerical oscillations due to the huge variations in small regions.

The conclusion is that the model requires the degradation term in order to converge. This term acts as a stabilization parameter, such that the Wnt concentration decreases monotonically until $x = 0$ and we do not see any abrupt transitions.

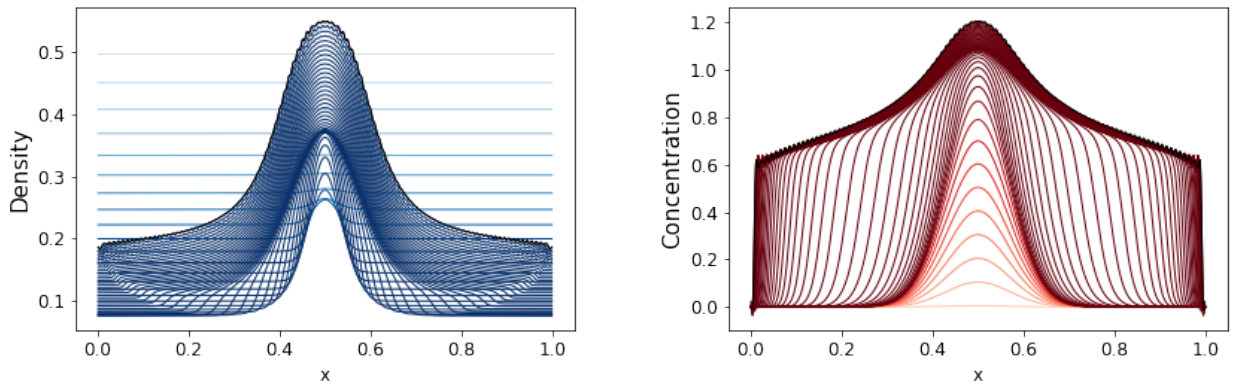

Figure 12: Cell density and Wnt concentration in the absence of degradation. A shock wave is formed near $x = 0$ in the Wnt concentration plot.

4.6 Cell divisions, cell extrusions and Wnt generation

There are two parameters which play a determinant role in deciding the behaviour of the system, δ_1 and δ_3. The first one is related to the ratio between extrusions and cell divisions, and the second one is related to the ratio between Wnt generation and cell divisions. A high value for δ_1 means that cell extrusions

occur at a higher rate than cell divisions, so the cell density decreases. On the other hand, small values of δ_1 imply that cell divisions occur at a higher rate than cell extrusions, so the density increases. As for δ_3, a high value of this parameter indicates that Wnt is generated at a higher speed than cell divisions take place, so the overall effect is that the Wnt concentration increases, and consequently the cell density does as well. On the contrary, a small value of δ_3 indicates that Wnt is generated at a slower rate than cell divisions take place, so the Wnt concentration decreases and the density does as well.

δ_1 can be roughly estimated from experimental data, since we know the mean rate of cell divisions inside the crypt and the mean rate of cell extrusions in the villus (its value is around 1). However, we have no direct way to measure δ_3, since we have no information of the magnitude of the rate of Wnt generation. Hence, a wide range of values has to be considered to try to fit the results to experimental data.

The behaviour of the system may differ if we change these parameters. If δ_1 is large and δ_3 is small, we expect the system to converge towards a null density state, since extrusions are much more abundant than divisions and Wnt is generated at a very slow rate. On the contrary, if δ_1 is small and δ_3 is large, the system may diverge, because Wnt is generated at a very high rate and extrusions take place much slower than divisions. A priori, there are some stabilization terms which would prevent the density and concentration from increasing indefinitely (the degradation term for c and the dependence of $k_d(\rho, c)$ with respect to ρ), but in practice numerical oscillations appear and the system may diverge. For an intermediate range of values, the cell density converges towards a non-trivial state.

Fig. 14 shows the behaviour of the system for different sets of parameters δ_1 and δ_3. The four colors correspond to:

- Red: The system diverges (the concentration tends to infinity and numerical oscillations appear).
- Green: The system converges towards an homeostatic equilibrium state with density different from zero.
- Yellow: The system converges towards an homeostatic equilibrium state with zero density.
- Grey: The results from simulations are inconclusive.

We can observe a very clear tendency in the behaviour of the system. As expected, the system diverges when δ_1 is small but δ_3 is large, and it tends to zero when δ_1 is large and δ_3 is small. There is a range of intermediate values which are the appropriate ones in order to get convergence towards a non-zero equilibrium state.

It is interesting to notice that for some values of δ_1 and δ_3 the results are not conclusive. This happens when the density takes very small values but not equal to zero. In those cases the system does not converge, although the error remains bounded, and numerical oscillations appear at the center of the crypt. Most of these states present very small cell densities, so we expect them to converge towards zero if smaller steps are used, or stabilization techniques are used.

Another important result is that, when we have convergence towards a non-trivial state, the cell density at the villus may go to zero (situation similar to the one found for very small ϵ). This can be seen in Fig. 13 (b). That is, we have two possible situations. On the first one, the cells are advected towards the villus and the density in that region is positive in the homeostatic equilibrium state. On the other hand, in some cases the cell density at the villus is zero because the cells are extruded very fast in comparison to the speed at which they are advected, and they do not reach the whole villus before being extruded. The second case happens when δ_3 is small compared to δ_1, so the rate of generation of Wnt is small compared to the extrusion rate.

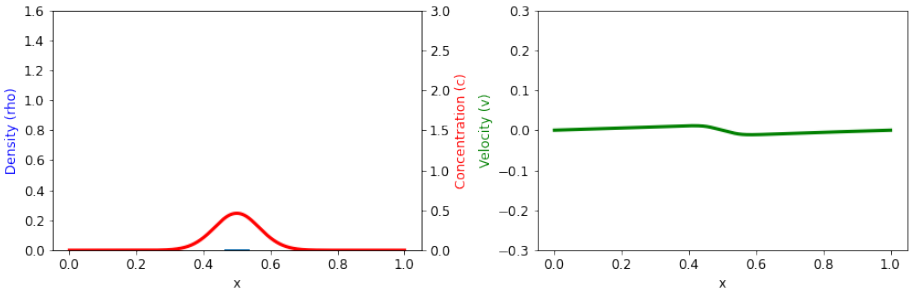

(a) $\delta_1 = 0.6$, $\delta_3 = 0.5$.

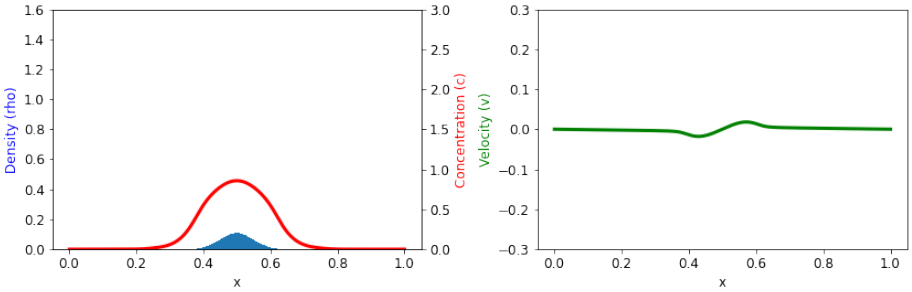

(b) $\delta_1 = 1.4$, $\delta_3 = 1.5$.

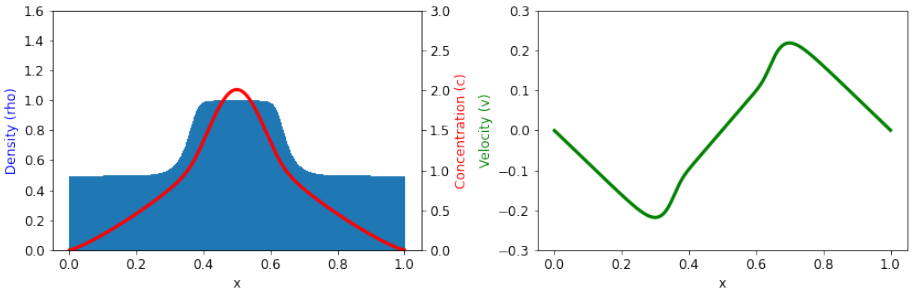

(c) $\delta_1 = 0.8$, $\delta_3 = 3$.

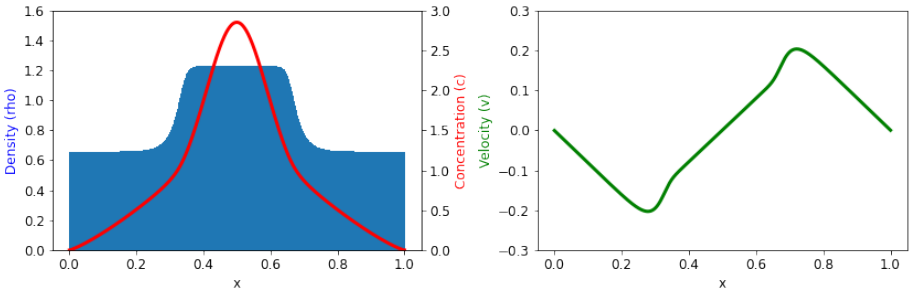

(d) $\delta_1 = 0.8$, $\delta_3 = 4$.

Figure 13: Cell density and Wnt concentration at the homeostatic equilibrium state under different values of δ_1 and δ_3.

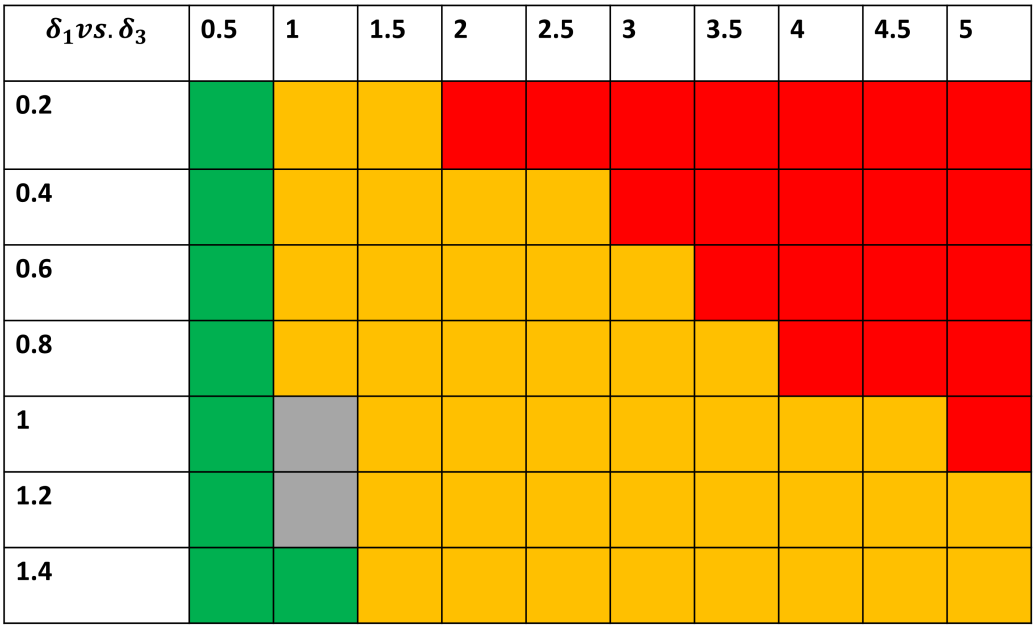

Figure 14: Analysis of convergence with respect to δ_1 (vertical) and δ_3 (horizontal).

5. Conclusions

The most remarkable conclusion from our project is that, starting from reasonable assumptions about the mechanics of the intestinal organoid and the dynamics of cell fate controlled by a morphogen, we have been able to develop a minimal model which captures the most important features of self-organized homeostatic steady states in intestinal organoids. Some of these features are a the division in two regions, the crypt and the villus. The crypt is characterized by a large density of cells, while the villus has a smaller density than the crypt. We also found a velocity pattern which drags the cells outside of the crypt, and a division-extrusion pattern divided in two regions: the crypt, where only cell divisions take place, and the villus, where extrusion take place.

From a mathematical point of view, the model consists on a system of partial differential system. Two of the equations involve derivatives in time of two of the variables, ρ and c, and the third equation only involves spatial derivatives. A remarkable fact is that we do not need to model the paneth cell density, nor any other signaling pathway besides Wnt, such as Notch, to reproduce experimental results with our model. We can assume that the dynamics of the paneth cells are negligible compared to the dynamics of enterocytes, and no other signaling pathway plays a key role in the system.

From a numerical point of view, the system is easy to solve using finite elements, since we could use a set of basis functions of order three, and we could use a simple first order time integrator. Some numerical oscillations appear in some cases, specially when the density takes very small values or when it increases very much, but in most cases these issues can be solved simply by decreasing the time step, considering an adaptative step size or increasing the degree of interpolation. Numerical stabilization techniques (such as GLS, ...) can also be considered to eliminate some of the stability issues.

We have verified that the model is robust with respect to initial conditions, as it reaches the same steady-state regardless of them. We have also established a parameter space where this state forms, as

well as how its features depend on key adimensional parameters. We have also provided physical insight in the effect of each of this parameters and determined their relevancy to the final state.

This work provides a framework to quantitatively understand homeostasis in rapidly renewing tissues, and to control tissue dynamics in vitro via intestinal organoids. This can be used to assist the design of bionic devices combining artificial and biological materials.

6. Future work

Now that the system has been verified and we know it works, the following step would be to apply this to a two dimensional case which can reproduce an actual intestinal organoid. The idea is to verify that the system self organizes in the same way as in one dimension and generated the same two separate regions, the villus and the crypt.

Another improvement for the system can be to add the dynamic of the Paneth cells to the model. This would require adding an extra equation for the Paneth cells density. Moreover, the Wnt generation rate is directly related to this density, so we would also have to modify the transport equation for the Wnt concentration. From a numerical point of view this can be quite challenging, since the Paneth cells dynamics are much slower than the enterocytes dynamics, so small time steps would be required to properly reproduce the enterocytes dynamics, but we would have to integrate over long periods of time in order to observe the Paneth cells dynamics.

Finally, a similar model can be deduced to model other organoids which are also regulated by signaling pathways similar to the Wnt. A study of these systems should be performed before hand, but a similar model could be obtained and many of the results found in this thesis could be useful to study similar systems.

A. Extra terms in the momentum equation

There are some extra terms we can add to the momentum balance equation (Eq. 3), using some biological arguments. For instance, we can define an energy characterising the repulsion between different cell types (mediated through Eph-Ephrin), which we could characterise by the gradient of c:

$$\mathcal{F}_{\text{rep}} = \int_\Omega \frac{\gamma}{2}|\nabla c|^2 d\Omega, \tag{33}$$

This would give rise to a tension

$$\sigma_{\text{rep}} = \frac{\gamma}{2}|\nabla c|^2. \tag{34}$$

We could also add another energy to characterise the mismatch of cell heights,

$$\mathcal{F}_{\text{mis}} = \int_\Omega \frac{L}{2}|\nabla \rho|^2 d\Omega, \tag{35}$$

$$\sigma_{\text{mis}} = \frac{L}{2}|\nabla \rho|^2 - L\rho\Delta\rho. \tag{36}$$

Indeed:

$$\frac{d}{dt}\mathcal{F}_{\text{rep}} = \int_\Omega \left[\frac{d}{dt} f_{rep} + \nabla\cdot(f_{rep}\mathbf{v})\right] d\Omega = \int_\Omega \left[\gamma\nabla c\nabla c_t + \nabla f_{rep}\cdot\mathbf{v} + f\nabla\cdot\mathbf{v}\right] d\Omega$$

Applying integration by parts to the last term yields:

$$\frac{d}{dt}\mathcal{F}_{\text{rep}} = \int_\Omega \left[\gamma\nabla c\cdot\nabla(k_p - \frac{1}{2}k_d c - \nabla c\cdot\mathbf{v}) + \nabla f_{rep}\cdot\mathbf{v} - \nabla f_{rep}\cdot\mathbf{v}\right] d\Omega$$

$$\frac{d}{dt}\mathcal{F}_{\text{rep}} = \int_\Omega -\gamma\nabla c\cdot\nabla(\nabla c\cdot\mathbf{v})d\Omega = \int_\Omega \gamma\nabla\cdot(\nabla c)\nabla c\cdot\mathbf{v}d\Omega = \int_\Omega \nabla\cdot(\frac{\gamma}{2}|\nabla c|^2\mathbf{I})\cdot\mathbf{v}d\Omega$$

This leads to the final expression in Eq. 34. Analogously,

$$\frac{d}{dt}\mathcal{F}_{\text{mis}} = \int_\Omega \left[\frac{d}{dt} f_{mis} + \nabla\cdot(f_{mis}\mathbf{v})\right] d\Omega = \int_\Omega \left[L\nabla\rho\nabla\rho_t + \nabla f_{mis}\cdot\mathbf{v} + f\nabla\cdot\mathbf{v}\right] d\Omega$$

Applying integration by parts to the last term yields:

$$\frac{d}{dt}\mathcal{F}_{\text{mis}} = \int_\Omega \left[L\nabla\rho\cdot\nabla(k_d(c)\rho - k_e(c)\rho - \nabla\cdot(\rho\mathbf{v})) + \nabla f_{mis}\cdot\mathbf{v} - \nabla f_{mis}\cdot\mathbf{v}\right] d\Omega$$

$$\frac{d}{dt}\mathcal{F}_{\text{mis}} = \int_\Omega -L\nabla\rho\cdot\nabla(\nabla\cdot(\rho\mathbf{v}))d\Omega = \int_\Omega L\nabla\cdot(\nabla\rho)\nabla\cdot(\rho\mathbf{v})d\Omega$$

$$\frac{d}{dt}\mathcal{F}_{\text{mis}} = \int_\Omega \left[L\nabla\cdot(\nabla\rho)\nabla\rho\cdot\mathbf{v} + L\nabla\cdot(\nabla\rho)\rho\nabla\cdot\mathbf{v}\right] d\Omega$$

$$\frac{d}{dt}\mathcal{F}_{\text{mis}} = \int_\Omega \left[\nabla\cdot(\frac{L}{2}|\nabla\rho|^2\mathbf{I})\cdot\mathbf{v} - \nabla\cdot(L\nabla\cdot(\nabla\rho)\rho\mathbf{I})\cdot\mathbf{v}\right] d\Omega$$

This leads to the final expression in Eq. 36.

These two term do not need to be considered a priori in the model. However, they can be useful to solve some issues which may appear in simulations. In particular, they are related to the smoothness of c and ρ.

B. Adaptative stepsize

One of the main issues in time integration is the choice of the time step. A large step may provoke numerical oscillations, and eventually make the method diverge. However, a time step which is too small would require a lot of iterations to converge to the equilibrium state. In the end, an intermediate time step must be selected to obtain the equilibrium state in a reasonable amount of iterations.

Many methods have been developed in the literature to treat this problem. One of them is considering an **adaptative stepsize** [17]. The idea of these kind of methods is to consider large time steps when we are far away from the equilibrium and small time steps when we are in a neighbourhood of the equilibrium state.

Let's assume we have an ODE of the form $\dot{y} = f(y, x)$, where $x \in \mathbb{R}^N$, and a first order Runge-Kutta method of the form: $y_{n+1} = y_n + b_1 \cdot k_1 + O(h^2)$. We can compute the error at iteration $n+1$ as $\Delta = y_{n+1} - y^*_{n+1}$. We want to make sure that the error is bounded, that is, $|\Delta| = |y_{n+1} - y^*_{n+1}| \leq scale$, where $scale = atol + |y| rtol$. Here, $atol$ is the absolute error tolerance and $rtol$ is the relative error tolerance. In practice, $max(|y_n|, |y_{n+1}|)$ is used for $|y|$ in the above formula, in case one of them is close to zero.

Δ is actually a vector of desired accuracies of length N, so in practice a norm of this vector is considered (for instance, the euclidean norm). We define:

$$err = \sqrt{\frac{1}{N} \sum_{i=0}^{N-1} \left(\frac{\Delta_i}{scale_i} \right)^2}$$

We accept the error if $err \leq 1$, and reject it otherwise.

The key point is the relation between err and h. Since the method is of first order, Δ scales as h^2, and so does err. Hence, if we take a step h_1 and produce an error err_1, the step h_0 that would have given some other value err_0 is readily estimated as:

$$h_0 = h_1 \left| \frac{err_0}{err_1} \right|^{1/2}$$

This gives us an estimate of how much we can increase or decrease the step size. The strategy is the following: if err at a given step size is greater than 1, we know how much we have to decrease the step size in order to guarantee convergence (that is, $err < 1$). On the other hand, if err is less than 1, we have an estimation on how much we can increase the step size keeping $err < 1$.

In the case of our model, we can compute the error as:

$$\Delta = \sqrt{\frac{1}{2} \left(\left(\frac{\rho_{n+1} - \rho_n}{atol_\rho + |\rho| rtol_\rho} \right)^2 + \left(\frac{c_{n+1} - c_n}{atol_c + |c| rtol_c} \right)^2 \right)}$$

Observe that we only include the error coming from ρ and c, but not from v. This is because v has no derivatives in time in the model, so changing the time step does not have any effect in the computation of v.

References

[1] C. Pérez-González, G. Ceada, F. Greco, M. Matejčić, M. Gómez-González, N. Castro, A. Menendez, S. Kale, D. Krndija, A. G. Clark, et al., Mechanical compartmentalization of the intestinal organoid enables crypt folding and collective cell migration, Nature cell biology 23 (7) (2021) 745–757.

[2] U. Alon, An introduction to systems biology: design principles of biological circuits, Chapman and Hall/CRC, 2006.

[3] M. Spit, B.-K. Koo, M. M. Maurice, Tales from the crypt: intestinal niche signals in tissue renewal, plasticity and cancer, Open Biol. 8 (9) (Sep. 2018).

[4] C. Pérez-González, G. Ceada, M. Matejčić, X. Trepat, Digesting the mechanobiology of the intestinal epithelium, Curr. Opin. Genet. Dev. 72 (2021) 82–90.

[5] L. Ritsma, S. I. Ellenbroek, A. Zomer, H. J. Snippert, F. J. De Sauvage, B. D. Simons, H. Clevers, J. Van Rheenen, Intestinal crypt homeostasis revealed at single-stem-cell level by in vivo live imaging, Nature 507 (7492) (2014) 362–365.

[6] H. J. Snippert, L. G. Van Der Flier, T. Sato, J. H. Van Es, M. Van Den Born, C. Kroon-Veenboer, N. Barker, A. M. Klein, J. Van Rheenen, B. D. Simons, et al., Intestinal crypt homeostasis results from neutral competition between symmetrically dividing lgr5 stem cells, Cell 143 (1) (2010) 134–144.

[7] C. Lopez-Garcia, A. M. Klein, B. D. Simons, D. J. Winton, Intestinal stem cell replacement follows a pattern of neutral drift, Science 330 (6005) (2010) 822–825.

[8] J. Guiu, E. Hannezo, S. Yui, S. Demharter, S. Ulyanchenko, M. Maimets, A. Jørgensen, S. Perlman, L. Lundvall, L. S. Mamsen, et al., Tracing the origin of adult intestinal stem cells, Nature 570 (7759) (2019) 107–111.

[9] M. Krausova, V. Korinek, Wnt signaling in adult intestinal stem cells and cancer, Cellular signalling 26 (3) (2014) 570–579.

[10] A. Gregorieff, J. L. Wrana, Seeing is believing: Wnt3 localization in the gut epithelium, Cell Research 26 (5) (2016) 515–516.

[11] Q. Xu, G. Mellitzer, V. Robinson, D. G. Wilkinson, In vivo cell sorting in complementary segmental domains mediated by eph receptors and ephrins, Nature 399 (6733) (1999) 267–271.

[12] J. Garcia-Ojalvo, Physical approaches to the dynamics of genetic circuits: a tutorial, Contemporary Physics 52 (5) (2011) 439–464.

[13] E. Latorre, S. Kale, L. Casares, M. Gómez-González, M. Uroz, L. Valon, R. V. Nair, E. Garreta, N. Montserrat, A. Del Campo, et al., Active superelasticity in three-dimensional epithelia of controlled shape, Nature 563 (7730) (2018) 203–208.

[14] M. Doi, Onsager's variational principle in soft matter, Journal of Physics: Condensed Matter 23 (28) (2011) 284118.

[15] H. Wang, T. Qian, X. Xu, Onsager's variational principle in active soft matter, Soft Matter 17 (13) (2021) 3634–3653.

[16] T. B. Saw, A. Doostmohammadi, V. Nier, L. Kocgozlu, S. Thampi, Y. Toyama, P. Marcq, C. T. Lim, J. M. Yeomans, B. Ladoux, Topological defects in epithelia govern cell death and extrusion, Nature 544 (7649) (2017) 212–216.

[17] P. Frolkovič, Numerical recipes: The art of scientific computing (1990).